A State-Space Approach to Intermodulation Distortion Estimation in Fully Balanced Bandpass G_m–C Filters With Weak Nonlinearities

Abdullah Çelik, *Student Member, IEEE*, Zhaonian Zhang, *Student Member, IEEE*, and Paul P. Sotiriadis, *Member, IEEE*

***Abstract*—A state-space approach to estimating intermodulation distortion in bandpass G_m–C filters with fully balanced, weakly nonlinear transconductors is introduced. It results in compact analytic expressions applicable to G_m–C filters of any order. For verifying the theory, two G_m–C filters with fully balanced weakly nonlinear transconductors have been designed using Cadence. They have been simulated in SpectreS as well as modeled and simulated in Simulink. Theory and simulation results are found in good agreement.**

***Index Terms*—Bandpass, circuit analysis, continuous-time filter, distortion model, fast algorithm, fully balanced, fully differential, G_m–C filter, intermodulation distortion (IMD), perturbation, state-space model, weak nonlinearity.**

I. Introduction

OVER the past few decades, continuous-time active filters [1] have emerged in a vast variety of applications and significant effort has been devoted to optimizing them.

G_m–C filters is one of the most popular classes of continuous-time filters. The basic building block of G_m–C filters is the integrator, typically realized by a linear transconductor and a capacitor as shown in Fig. 1. Early implementations were done in bipolar technology [2], [3] but the advances in CMOS technologies provided the ideal ground for them [33].

G_m–C filters, like all active filters, exhibit some nonlinear behavior that is primarily due to the nonlinearity of their active elements, i.e., the transconductors, and introduces distortion to the signal. This work focuses *on intermodulation* distortion that is particularly important in characterizing nonlinearity in bandpass filters. Bandpass G_m–C filters are used in many applications like wireless communication where their nonlinearity (and noise) determines the performance of the whole system. By their nature, (narrow) bandpass filters suffer mainly from intermodulation distortion (IMD) and in most practical cases by the third-order IMD (IM_3).

IMD is the set of cross-product signals that are generated when two or more sinusoidal signals (beats) are present at the input of a non (perfectly) linear circuit. These spurious products are mathematically related to the original input signals. The standard test input signal for IMD estimation is composed of two beats at frequencies f_1 and f_2; and, it results in intermodulation products (IMPs) at frequencies[1] $\pm Mf_1 \pm Nf_2$, where $M, N = 1, 2, 3, \ldots$. The sum $M + N$ is called the *order* of the IMP, e.g., the second-order IMPs occur at frequencies $f_1 + f_2$ and $f_2 - f_1$; the third-order IMPs appear at $2f_1 + f_2, 2f_1 - f_2, f_1 + 2f_2$, and $f_1 - 2f_2$, and so on. Typically in a bandpass filter (or system in general) the IMPs that are dominant and usually important for the performance of the filter are the ones occurring at frequencies within its passband. In standard IMD two-beat tests, f_1 and f_2 are very close to each other and the IMPs that pass through the filter are at $(M+1)f_1 - Mf_2$ and $(M+1)f_2 - Mf_1$ for small values of $M = 1, 2, 3, \ldots$. Moreover, typically in weakly nonlinear filters the magnitude of the IMPs drops rapidly with their order. Because of that, in almost all practical cases, IMD analysis and measurements in bandpass filters focus on the third-order IMP at $2f_1 - f_2$ [16], [17]. Note that the IMP at $2f_2 - f_1$ behaves similarly since $f_1 \approxeq f_2$.

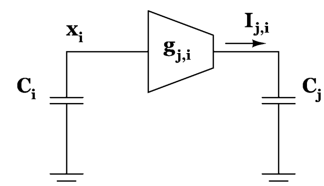

Fig. 1. Transconductor model.

The most popular metric of third-order IMD (IM_3) is the ratio of third-order IMP at frequency $2f_1 - f_2$ over the amplitude of the (desirable) signal at f_1, i.e., IM_3 is defined relatively to the beat at f_1, [9], [16]. Related measures of IM_3, mainly in RF amplifiers, are the third-order intercept point (IP_3), the 1-dB compression point $(P_{1\,\mathrm{dB}})$, and the spurious-free dynamic range (SFDR), e.g., [6]–[8] and [16].

Some circuits realize static (memoryless) input-output functions and IMD estimation can be done at the transistor level using algebraic techniques [26], [27], [17], [9]. This approach is complemented by circuit techniques that enhance the linearity of amplifying stages e.g., [5], [11], [12], [25].

Filters on the other hand are dynamical systems (they have memory) which makes their IMD estimation a more complicated problem. Volterra series is the most popular tool to address it e.g., [13]–[15]. However, deriving analytical results is

[1]Throughout the paper, we do not distinguish between positive and negative frequencies.

Manuscript received September 24, 2005; revised April 12, 2006 and August 11, 2006. This paper was recommended by Associate Editor G. Palumbo.

A. Çelik was with the Department of Electrical Engineering, The Johns Hopkins University, Baltimore, MD 21218 USA. He is now with MAXIM Integrated Products, Sunnyvale, CA 94086 USA.

P. P. Sotiriadis and Z. Zhang are with the Department of Electrical Engineering, The Johns Hopkins University, Baltimore, MD 21218 USA (e-mail: pps@jhu.edu).

Digital Object Identifier 10.1109/TCSI.2006.887630

practically possible only in low-order or specially structured filters (systems). A variant of the Volterra series approach for frequency-domain analysis of weakly nonlinear circuits has been presented in [28]. In most cases the Volterra series methods lead to complicated algebraic expressions. However, in feedback amplifiers, exhibiting weak nonlinearity, the (harmonic) distortion[2] has been derived analytically without involving complicated Voltera series analysis [29]. This, is done assuming static tranconductance nonlinearity, and, provides useful guidelines in optimizing the designs of the amplifier and feedback network [30]–[32].

An alternative frequency-domain approach for general G_m–C filters was introduced in [18] where the total IMD product of the filter is approximated by the sum of the IMD products of the individual transconductors, linearly propagated to the output of the filter through the corresponding partial transfer functions.

The work presented in this paper was motivated by the need for a low-complexity IMD estimation method that results in analytical expressions valid for G_m–C filters of any order and topology. In contrast to existing techniques, this paper introduces a *state-space* approach to IMD estimation which is applied to G_m–C filters. This new approach leads to analytic expressions that explicitly depend on the structural matrices of the filter and its component values providing a simple and very general tool for the estimation of IMD. The resulting formulas are independent of the order and the topology of the filter. Validation of the developed theory has been done by the design of two G_m–C filters in a 0.5-μm standard CMOS process using Cadence, simulation in SpectreS, and in addition by modeling and simulation of the filters in Simulink. The simulation and theoretical results were found in good agreement.

The paper is organized as follows: Section II introduces the definitions, assumptions, notation and state-space modeling of the weakly nonlinear G_m–C filters. Section III presents a decomposition of the filter and the derivation of IM_3. Section IV presents the simulation's setup and results, and the comparison between the theory and simulation results. Appendix D summarizes the IMD derivation as an algorithm that is very easily implemented in MATLAB.

II. Transconductor and G_m–C Filter Models

The mathematical models, state-space formulation, notation, and assumptions used throughout the paper are introduced in this section.

A. Fully Balanced Weakly Nonlinear Transconductors

In this work, we study G_m–C filters based on *fully balanced* transconductors with weak nonlinearity. The motivation for doing so results from the fact that fully balanced (differential) transonductors are almost always preferred in low-distortion linear circuits, such as filters, due to their significantly higher linearity [1], [3], [8], [33], [12]. For convenience, however, we use the single-ended notation in Fig. 1. The subscripts of the gain, $g_{j,i}$, and current, $I_{j,i}$, indicate that the input is connected to node i and the output is connected to node j.

[2]Tools for deriving harmonic distortion sometimes apply to the derivation of IMD and vice versa.

Because of its balanced structure a fully differential (balanced) transconductor exhibits mainly *odd*-order nonlinearity and so $I_{j,i}$ can be expressed as: $I_{j,i} = g_{j,i}x_i + e_{j,i}x_i^3 + k_{j,i}{x_i}^5 + \cdots$. Also, in most practical cases, the fifth and higher order terms are negligible compared to the third-order term and can be safely ignored, i.e.,

$$I_{j,i} = g_{j,i}x_i + e_{j,i}x_i^3. \tag{1}$$

These assumptions are typical in estimating the distortion of filters with fully balanced transconductors [14], [18] and are adopted here as well. Moreover, in many practical cases the coefficient of the third power, $e_{j,i}$, is proportional to $g_{j,i}$, i.e., $e_{j,i} = \alpha g_{j,i}$. This condition is used in the paper to reduce algebraic complexity although the theory is applicable to the more general case (see footnote in Section II-C and Appendix A). It gives

$$I_{j,i} = g_{j,i}x_i + \alpha g_{j,i}x_i^3. \tag{2}$$

The transconductance $g_{j,i}$ and the (small) constant α, which has units of Volt^{-2}, can be derived *analytically* (Appendix A) or *numerically* by fitting a third-order polynomial to the $I-V$ characteristic of the transconductor.

B. Example: State-Space Model of Second-Order Fully Balanced G_m–C Filter With Weak Third-Order Nonlinearity

The theoretical development in the paper is based on state-space representation of G_m–C filters in the form of a linear (finite dimensional) dynamical systems

$$\begin{aligned}\dot{\mathbf{x}}(t) &= \mathbf{A}\mathbf{x}(t) + \mathbf{b}u(t)\\ y(t) &= \mathbf{c}^T\mathbf{x}(t) + du(t).\end{aligned}$$

The state vector $\mathbf{x}(t)$ is in $\Re^n$ and its entries are the voltages of the capacitors in the G_m–C filter. Matrices $\mathbf{A}, \mathbf{b}, \mathbf{c}$, and d are $n \times n, n \times 1, n \times 1$, and 1×1 respectively. Since d only replicates the input at the output, it is omitted without loss of generality.

Consider the bandpass G_m–C filter in Fig. 2 for example. The state-space formulation of the filter is given by the following system of differential equations

$$\underbrace{\begin{bmatrix}\dot{x}_1(t)\\ \dot{x}_2(t)\end{bmatrix}}_{\dot{\mathbf{x}}(t)} \; = \; \underbrace{\begin{bmatrix}\frac{g_{1,1}}{C_1} & \frac{g_{1,2}}{C_1}\\ \frac{g_{2,1}}{C_2} & 0\end{bmatrix}}_{\mathbf{A}} \underbrace{\begin{bmatrix}x_1(t)\\ x_2(t)\end{bmatrix}}_{\mathbf{x}(t)} + \underbrace{\begin{bmatrix}\frac{g_{1,I}}{C_1}\\ 0\end{bmatrix}}_{\mathbf{b}} u(t) \tag{3}$$

and the output algebraic equations:

$$y(t) = \underbrace{\begin{bmatrix}g_{o,1} & 0\end{bmatrix}}_{\mathbf{c}^T} \underbrace{\begin{bmatrix}x_1\\ x_2\end{bmatrix}}_{\mathbf{x}(t)} \tag{4}$$

Also, in this work, the input u is the standard two-beat signal used in IMD estimation

$$u(t) = k_1\sin(w_1 t) + k_2\sin(w_2 t). \tag{5}$$

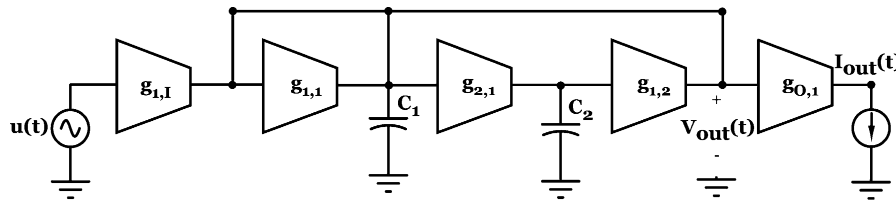

Fig. 2. Second-order bandpass G_m–C filter.

The weak third-order nonlinearity of the transconductors is taken into account by incorporating expression (2), of the transconductors' output currents, into (3) and (4). So

$$\underbrace{\begin{bmatrix}\dot{x}_1(t)\\ \dot{x}_2(t)\end{bmatrix}}_{\dot{\mathbf{x}}(t)} = \underbrace{\begin{bmatrix}\frac{g_{1,1}}{C_1} & \frac{g_{1,2}}{C_1}\\ \frac{g_{2,1}}{C_2} & 0\end{bmatrix}}_{\mathbf{A}} \underbrace{\begin{bmatrix}x_1(t)\\ x_2(t)\end{bmatrix}}_{\mathbf{x}(t)} + \underbrace{\alpha\begin{bmatrix}\frac{g_{1,1}}{C_1} & \frac{g_{1,2}}{C_1}\\ \frac{g_{2,1}}{C_2} & 0\end{bmatrix}}_{\alpha\mathbf{A}} \underbrace{\begin{bmatrix}x_1^3(t)\\ x_2^3(t)\end{bmatrix}}_{\mathbf{x}^{\bullet 3}(t)} + \underbrace{\begin{bmatrix}\frac{g_{1,I}}{C_1}\\ 0\end{bmatrix}}_{\mathbf{b}} u(t) + \underbrace{\alpha\begin{bmatrix}\frac{g_{1,I}}{C_1}\\ 0\end{bmatrix}}_{\alpha\mathbf{b}} u^3(t) \tag{6}$$

$$y(t) = \underbrace{[g_{o,1} \quad 0]}_{\mathbf{c}^T} \underbrace{\begin{bmatrix}x_1(t)\\ x_2(t)\end{bmatrix}}_{\mathbf{x}(t)} + \underbrace{\alpha\,[g_{o,1} \quad 0]}_{\alpha\mathbf{c}^T} \underbrace{\begin{bmatrix}x_1^3(t)\\ x_2^3(t)\end{bmatrix}}_{\mathbf{x}^{\cdot 3}(t)}. \tag{7}$$

Hadamard's product is used in the formulation above: for any two k-dimensional vectors $\mathbf{a} = (a_1, a_2, \ldots, a_k)^T$ and $\mathbf{b} = (b_1, b_2, \ldots, b_k)^T$ their Hadamard product is defined as $\mathbf{a} \bullet \mathbf{b} = (a_1b_1, a_2b_2, \ldots, a_kb_k)^T$ and the Hadamard's ρth power is $\mathbf{a}^{\bullet\rho} = (a_1{}^{\rho}, a_2{}^{\rho}, \ldots, a_k{}^{\rho})^T$.

Note that in many G_m–C filters the output is a capacitor's voltage. In Fig. 2 for example, if we take x_2 as the output signal, then (there is no output transconductor and) expression (7) becomes $y = x_2$, *which is linear.*

C. State-Space Model of General nth-Order Fully Balanced G_m–C Filter With Weak Third-Order Nonlinearity

The state-space model of a general nth-order G_m–C filter is given by the system (8) and (9) below. The state variables are the capacitors' voltages x_1 to x_n

$$\underbrace{\begin{bmatrix}\dot{x}_1(t)\\ \dot{x}_2(t)\\ \vdots\\ \dot{x}_n(t)\end{bmatrix}}_{\dot{\mathbf{x}}(t)} = \underbrace{\begin{bmatrix}\frac{g_{1,1}}{C_1} & \frac{g_{1,2}}{C_1} & \cdots & \frac{g_{1,n}}{C_1}\\ \frac{g_{2,1}}{C_2} & \frac{g_{2,2}}{C_2} & \cdots & \frac{g_{2,n}}{C_2}\\ \vdots & \vdots & \ddots & \vdots\\ \frac{g_{n,1}}{C_n} & \frac{g_{n,2}}{C_n} & \cdots & \frac{g_{n,n}}{C_n}\end{bmatrix}}_{\mathbf{A}} \underbrace{\begin{bmatrix}x_1(t)\\ x_2(t)\\ \vdots\\ x_n(t)\end{bmatrix}}_{\mathbf{x}(t)} + \underbrace{\begin{bmatrix}\frac{g_{1,I}}{C_1}\\ \frac{g_{2,I}}{C_2}\\ \vdots\\ \frac{g_{n,I}}{C_n}\end{bmatrix}}_{\mathbf{b}} \underbrace{u(t)}_{u(t)} \tag{8}$$

and

$$\underbrace{\begin{bmatrix}y_1(t)\\ y_2(t)\\ \vdots\\ y_n(t)\end{bmatrix}}_{y(t)} = \underbrace{[g_{o,1} \quad g_{o,2} \quad \cdots \quad g_{o,n}]}_{\mathbf{c}^T} \underbrace{\begin{bmatrix}x_1(t)\\ x_2(t)\\ \vdots\\ x_n(t)\end{bmatrix}}_{\mathbf{x}(t)}. \tag{9}$$

The state-space model for the general fully balanced nth-order G_m–C filter with weak third-order nonlinearity is derived by combining (8) and (9) with (2). It is[3]

$$\dot{\mathbf{x}}(t) = \mathbf{A}\mathbf{x}(t) + \alpha\mathbf{A}\mathbf{x}^{\bullet 3}(t) + \mathbf{b}u(t) + \alpha\mathbf{b}u^3(t) \tag{10}$$

$$y(t) = \mathbf{c}^T\mathbf{x}(t) + \alpha\mathbf{c}^T\mathbf{x}^{\bullet 3} \tag{11}$$

where $\mathbf{A} \in \Re^{n\times n}, \mathbf{x}, \mathbf{b}, \mathbf{c} \in \Re^{n\times 1}$ and $u(t), y(t) \in \Re$. Again, "$\bullet$" stands for Hadamard product.

Finally, in certain high-Q bandpass G_m–C, filters we may have to take into account the parasitic output impedance of the transconductors in order to accurately estimate the frequency response of the filter. The parasitic output impedance is typically modelled as a parallel $R - C$. The capacitor can be incorporated into the filter's node capacitor. The resistor, R, can be modeled as another transconductor whose input and output are connected to this node. The weakly nonlinear transconductor model, (2), introduced above can be used; assuming that R is relatively large, the weak nonlinearity should not cause any significant error. This way, the system (10) and (11) remain valid.

III. G_m–C Filter's Structural Decomposition

Our state-space IMD estimation approach is based on: i) structural decomposition of the filter into a cascade of three (weakly nonlinear) stages; and, ii) derivation of the distortion introduced by each stage and linear propagation of it to the output. The principle resembles that in [18] but here we consider the stages instead of the transconductors as the basic elements introducing distortion.

The block diagram of the weakly nonlinear G_m–C filter, modeled by (10) and (11), is shown in Fig. 3. The filter (considered as a dynamical system) is viewed as a cascade of three stages: the input stage that corresponds to signal operator S_1, the filter core stage, operator S_2 and the output stage, operator S_3. It is

$$\mathbf{w} = S_1(u), \mathbf{x} = S_2(\mathbf{w}) \text{ and } y = S_3(\mathbf{x}).$$

The total response of the system is given by their composition $y = (S_3 \circ S_2 \circ S_1)(u)$.

Regarding S_1, S_2, and S_3 it is important to mention the following two facts.

1) Since this work focuses on the derivation of IMD with two-beats input signal $u(t) = k_1\sin(w_1t) + k_2\sin(w_2t)$,

[3] If there is no constant α such that $e_{j,i} = \alpha g_{j,i}$, in (1), then system (10) and (11) must be replaced by the more general ones $\dot{\mathbf{x}} = \mathbf{A}\mathbf{x} + \mathbf{E}\mathbf{x}^{\bullet 3} + \mathbf{b}u + \mathbf{h}u^3$ and $y = \mathbf{c}^T\mathbf{x} + \mathbf{q}^T\mathbf{x}^{\bullet 3}$, where $\mathbf{E}$, $\mathbf{h}$, and $\mathbf{q}$ are the corresponding matrices for the third-order nonlinear terms. Although the algebra is more involved in this case, the steps presented in this work can be followed exactly to derive the total distortion of the filter.

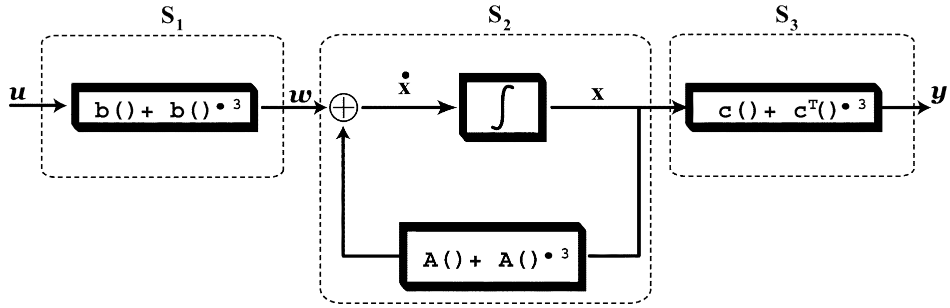

Fig. 3. Block diagram of the weakly nonlinear G_m–C filter.

only the steady-state behavior of the filter is taken into consideration. To this end, the (linear) filter is assumed asymptotically stable by design (i.e., all eigenvalues of matrix A have negative real parts) and operator S_2 maps signal w to the steady state, x, of the system.

2) Although the input and output stages S_1 and S_3 are static functions, and distortion due to static nonlinearities has been studied extensively, the filter core S_2 has dynamics making the IMD estimation problem more challenging.

To deal with operator S_2 *regular perturbation theory* is employed in Section III-D.

Each of the three stages[4] is naturally decomposed into two parts, the linear one (ideal) and the nonlinear one (representing the nonlinearity of the stage). We write

$$S_i = S_i^{\ell} + S_i^{n}, \qquad i = 1, 2, 3. \tag{12}$$

The decomposition of S_1 and S_3 is implied directly from Fig. 3, that is

$$\begin{aligned} S_1^{\ell}(u) &\triangleq \mathbf{b}u \quad S_1^{n}(u) \triangleq \alpha \mathbf{b} u^3 \\ S_3^{\ell}(\mathbf{x}) &\triangleq \mathbf{c}^T\mathbf{x} \quad S_3^{n}(\mathbf{x}) \triangleq \alpha \mathbf{c}^T \mathbf{x}^{\bullet 3}. \end{aligned} \tag{13}$$

The linear part S_2^{ℓ} of S_2 is the steady-state response of the (asymptotically stable) linear system $\dot{\mathbf{x}}_0 = \mathbf{A}\mathbf{x}_0 + \mathbf{w}$, i.e., $S_2^{\ell}(\mathbf{w}) = \mathbf{x}_0$ (steady state). Operator S_2^n is defined as $S_2^n \triangleq S_2 - S_2^{\ell}$ i.e., $\mathbf{x_d} = S_2^n(\mathbf{w})$ is the difference between the steady-state responses of the nonlinear and the linear systems shown in Fig. 4.

The decomposition of the stages (12) is shown in the block diagram of Fig. 5. The cascade in Fig. 5 from the input u to the output $y = (S_3 \circ S_2 \circ S_1)(u)$ of the filter, can be decomposed into eight *signal paths*,[5] namely $S_3^{\ell} \circ S_2^{\ell} \circ S_1^{\ell}, S_3^{\ell} \circ S_2^{\ell} \circ S_1^{n}, \ldots, S_3^{n} \circ S_2^{n} \circ S_1^{n}$ and the output signal is written as

$$\begin{aligned} y = &\left(S_3^{\ell} \circ S_2^{\ell} \circ S_1^{\ell}\right)(u) + \left(S_3^{\ell} \circ S_2^{\ell} \circ S_1^{n}\right)(u) \\ &+ \left(S_3^{\ell} \circ S_2^{n} \circ S_1^{\ell}\right)(u) + \left(S_3^{n} \circ S_2^{\ell} \circ S_1^{\ell}\right)(u) \\ &+ \left(S_3^{\ell} \circ S_2^{n} \circ S_1^{n}\right)(u) + \left(S_3^{n} \circ S_2^{\ell} \circ S_1^{n}\right)(u) \\ &+ \left(S_3^{n} \circ S_2^{n} \circ S_1^{\ell}\right)(u) + \left(S_3^{n} \circ S_2^{n} \circ S_1^{n}\right)(u). \end{aligned} \tag{14}$$

[4]From now on, each of the three stages is identified with its operator and the terms *stage* and *operator* are used indistinguishably.

[5]More discussion on the decomposition into these eight signal paths can be found in [34].

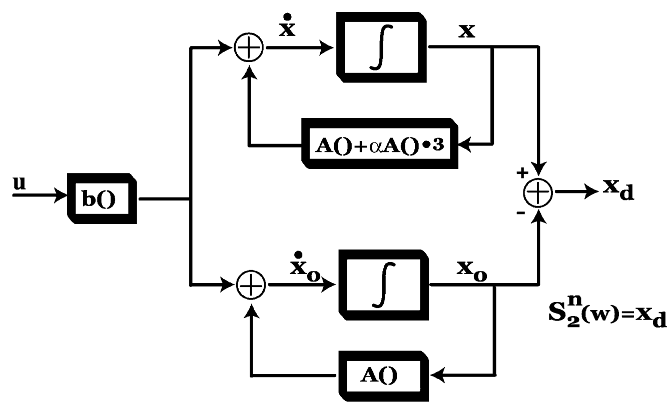

Fig. 4. Definition of operator S_2^n.

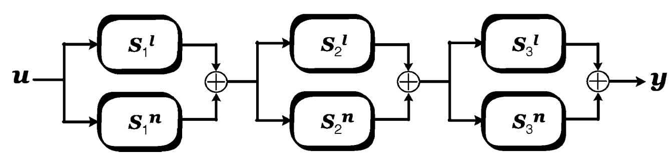

Fig. 5. Filter as a cascade of decomposed stages.

Each summand in (14), i.e., each signal path, is composed out of three operators. Since we consider only weakly nonlinear filters, it is expected that operators S_1^n, S_2^n, and S_3^n have a minor contribution to the output signal. All the more, *compositions* of two or three of the nonlinear operators S_1^n, S_2^n, or S_3^n in a signal path should result in a negligible signal component. Therefore, keeping only the signal paths with at most one nonlinear operator should result in a good approximation of the filter's behavior. In other words, from (14), we have

$$\begin{aligned} y \approxeq &\left(S_3^{\ell} \circ S_2^{\ell} \circ S_1^{\ell}\right)(u) + \left(S_3^{\ell} \circ S_2^{\ell} \circ S_1^{n}\right)(u) \\ &+ \left(S_3^{\ell} \circ S_2^{n} \circ S_1^{\ell}\right)(u) + \left(S_3^{n} \circ S_2^{\ell} \circ S_1^{\ell}\right)(u). \end{aligned} \tag{15}$$

Finally, the input signal is the two-beat $u(t) = k_1 \sin(w_1 t) + k_2 \sin(w_2 t)$, used for IMD estimation, and following the discussion in the introduction, we are interested in the IMD components at frequencies $2w_1 - w_2$ and $2w_2 - w_1$. Moreover, because of the symmetric form of u, only one of them is really needed. To this end, we focus only on the frequency components of y at w_1, w_2, and $2w_1 - w_2$. The following notation is used:

$$\hat{y} \triangleq \text{Sum of signal components of } y \text{ at frequencies } w_1, w_2 \text{ and } 2w_1 - w_2. \tag{16}$$

E.g., if $y(t) = 2\sin(w_1 t) + 3\cos(w_2 t) + 0.3\sin(3w_1) + 0.2\cos(2w_1 - w_2) + 0.1\cos(2w_2 - w_1) + 0.02\sin(5w_2)$,

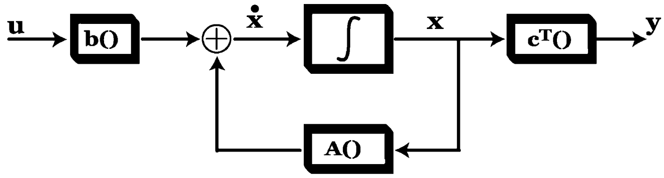

Fig. 6. Linear (ideal) system.

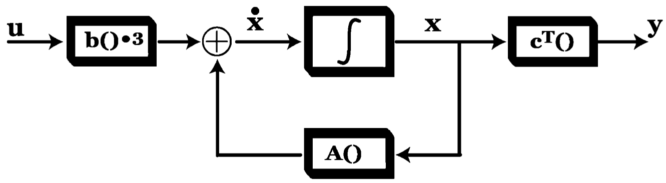

Fig. 7. Block diagram of input stage's nonlinearity.

then $\hat{y}(t) = 2\sin(w_1 t) + 3\cos(w_2 t) + 0.2\cos(2w_1 - w_2)$. To simplify notation we set

$$\Omega_{\boldsymbol{I}} \triangleq 2w_1 - w_2.$$

In the following sections, the contributions of the three stages to the total IMD are derived using (15) and (16). Specifically, the four dominant signal paths, i.e., $S_3^\ell \circ S_2^\ell \circ S_1^\ell, S_3^\ell \circ S_2^\ell \circ S_1^n, S_3^\ell \circ S_2^n \circ S_1^\ell$, and $S_3^n \circ S_2^\ell \circ S_1^\ell$ are studied. Finally note that the nonlinearity of the input and output stages is static and can be easily addressed. On the contrary, the nonlinearity of the filter core is dynamic and much more involved to analyze.

A. Ideal (Linear) System: Operator $S_3^\ell \circ S_2^\ell \circ S_1^\ell$

The first term, $S_3^\ell \circ S_2^\ell \circ S_1^\ell$, in expression (15) corresponds to the ideal (linear) filter shown in Fig. 6 with state-space representation

$$\begin{aligned}\dot{\mathbf{x}}(t) &= \mathbf{A}\mathbf{x}(t) + \mathbf{b}u(t)\\ y_{\ell\ell\ell}(t) &= \mathbf{c}^T\mathbf{x}(t).\end{aligned} \tag{17}$$

For input $u(t) = k_1\sin(w_1 t) + k_2\sin(w_2 t)$, the steady-state output signal $y_{\ell\ell\ell}$ is given by (18), where I is the $n \times n$ identity matrix. The details of the derivation are available in Appendix B [(56) and (57)]

$$\begin{aligned}y_{\ell\ell\ell}(t) = &-k_1\mathbf{c}^T\left(w_1^2\mathbf{I} + \mathbf{A}^2\right)^{-1} w_1\mathbf{b}\cos\left(w_1 t\right)\\ &- k_1\mathbf{c}^T\left(w_1^2\mathbf{I} + \mathbf{A}^2\right)^{-1}\mathbf{A}\mathbf{b}\sin\left(w_1 t\right)\\ &- k_2\mathbf{c}^T\left(w_2^2\mathbf{I} + \mathbf{A}^2\right)^{-1} w_2\mathbf{b}\cos\left(w_2 t\right)\\ &- k_2\mathbf{c}^T\left(w_2^2\mathbf{I} + \mathbf{A}^2\right)^{-1}\mathbf{A}\mathbf{b}\sin\left(w_2 t\right).\end{aligned} \tag{18}$$

B. Input Stage Nonlinearity: Operator $S_3^\ell \circ S_2^\ell \circ S_1^n$

The second term, $S_3^\ell \circ S_2^\ell \circ S_1^n$, in (15) models the distortion of the input transconductors and its propagation to the output of the filter, based on the approximations discussed in Section III. These are modeled by the block diagram in Fig. 7 and (19)

$$\begin{aligned}\dot{\mathbf{x}}(t) &= \mathbf{A}\mathbf{x}(t) + \alpha\mathbf{b}u^3(t)\\ y_{\ell\ell n}(t) &= \mathbf{c}^T\mathbf{x}(t).\end{aligned} \tag{19}$$

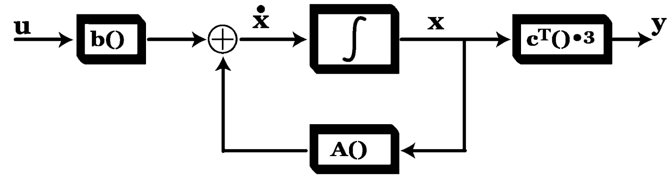

Fig. 8. Block diagram of output stage's nonlinearity.

By replacing $u^3(t) = (k_1\sin(w_1 t) + k_2\sin(w_2 t))^3$ into (19), solving the dynamical system and keeping only the steady-state output signal components at frequencies w_1, w_2, and $2w_1 - w_2$ we get $\hat{y}_{\ell\ell n}$ given by (20). The details can be found in Appendix B

$$\begin{aligned}\hat{y}_{\ell\ell n}(t) = &-\alpha\frac{3}{4}{k_1}^2 k_2\mathbf{c}^T\left(\Omega_{\boldsymbol{I}}^2\mathbf{I} + \mathbf{A}^2\right)^{-1}\mathbf{A}\mathbf{b}\sin\left(\Omega_{\boldsymbol{I}} t\right)\\ &- \alpha\frac{3}{4}{k_1}^2 k_2\mathbf{c}^T\left(\Omega_{\boldsymbol{I}}^2\mathbf{I} + \mathbf{A}^2\right)^{-1}\Omega_{\boldsymbol{I}}\mathbf{b}\cos\left(\Omega_{\boldsymbol{I}} t\right)\\ &- \alpha\left(\frac{3}{2}k_1{k_2}^2 + \frac{3}{4}{k_1}^3\right)\\ &\times\mathbf{c}^T\left({w_1}^2\mathbf{I} + \mathbf{A}^2\right)^{-1}\mathbf{A}\mathbf{b}\sin(w_1 t)\\ &- \alpha\left(\frac{3}{2}k_1{k_2}^2 + \frac{3}{4}{k_1}^3\right)\\ &\times\mathbf{c}^T\left({w_1}^2\mathbf{I} + \mathbf{A}^2\right)^{-1} w_1\mathbf{b}\cos(w_1 t)\\ &- \alpha\left(\frac{3}{2}{k_1}^2 k_2 + \frac{3}{4}{k_2}^3\right)\\ &\times\mathbf{c}^T\left({w_2}^2\mathbf{I} + \mathbf{A}^2\right)^{-1}\mathbf{A}\mathbf{b}\sin(w_2 t)\\ &- \alpha\left(\frac{3}{2}{k_1}^2 k_2 + \frac{3}{4}{k_2}^3\right)\\ &\times\mathbf{c}^T\left({w_2}^2\mathbf{I} + \mathbf{A}^2\right)^{-1} w_2\mathbf{b}\cos(w_2 t).\end{aligned} \tag{20}$$

C. Output Stage Nonlinearity: Operator $S_3^n \circ S_2^\ell \circ S_1^\ell$

The fourth term $S_3^n \circ S_2^\ell \circ S_1^\ell$ in expression (15) captures the distortion introduced by the output stage. The corresponding block diagram is shown in Fig. 8 and the dynamical system model is

$$\begin{aligned}\dot{\mathbf{x}}(t) &= \mathbf{A}\mathbf{x}(t) + \mathbf{b}u(t)\\ y_{n\ell\ell}(t) &= \alpha\mathbf{c}^T\mathbf{x}^{\bullet 3}(t).\end{aligned} \tag{21}$$

The steady-state solution $x(t)$ of system (21), for $u(t) = k_1\sin(w_1 t) + k_2\sin(w_2 t)$, is (Appendix B)

$$\begin{aligned}\mathbf{x}(t) = &\mathbf{h_1}\sin\left(w_1 t\right) + \mathbf{p_1}\cos\left(w_1 t\right)\\ &+ \mathbf{h_2}\sin\left(w_2 t\right) + \mathbf{p_2}\cos\left(w_2 t\right)\end{aligned} \tag{22}$$

where

$$\begin{aligned}\mathbf{h_1} &= -k_1\left(w_1^2\mathbf{I} + \mathbf{A}^2\right)^{-1}\mathbf{A}\mathbf{b}\\ \mathbf{p_1} &= -k_1\left(w_1^2\mathbf{I} + \mathbf{A}^2\right)^{-1} w_1\mathbf{b}\\ \mathbf{h_2} &= -k_2\left(w_2^2\mathbf{I} + \mathbf{A}^2\right)^{-1}\mathbf{A}\mathbf{b}\\ \mathbf{p_2} &= -k_2\left(w_2^2\mathbf{I} + \mathbf{A}^2\right)^{-1} w_2\mathbf{b}.\end{aligned} \tag{23}$$

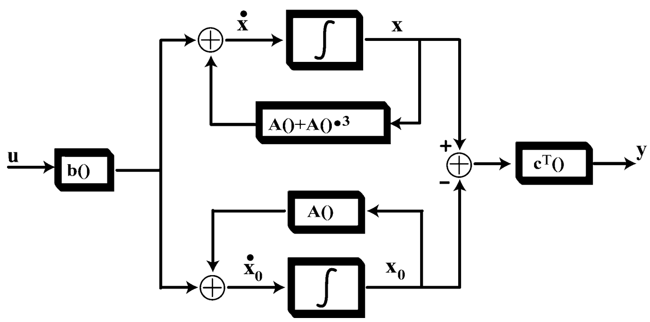

Fig. 9. Block diagram of filter core's nonlinearity.

Constants $\mathbf{h_1}, \mathbf{p_1}, \mathbf{h_2}$, and $\mathbf{p_2}$ depend linearly on amplitudes k_1 and k_2. It is convenient to define the corresponding constants without the amplitudes, (24), as well. Note that $\mathbf{h_1}, \mathbf{p_1}, \mathbf{h_2}, \mathbf{p_2}, \tilde{\mathbf{h}}_\mathbf{1}, \tilde{\mathbf{p}}_\mathbf{1}, \tilde{\mathbf{h}}_\mathbf{2}$, and $\tilde{\mathbf{p}}_\mathbf{2}$ are all real column vectors of size n

$$\begin{aligned}\tilde{\mathbf{h}}_\mathbf{1} &= -\left(w_1^2\mathbf{I}+\mathbf{A}^2\right)^{-1}\mathbf{Ab}\\ \tilde{\mathbf{p}}_\mathbf{1} &= -\left(w_1^2\mathbf{I}+\mathbf{A}^2\right)^{-1}w_1\mathbf{b}\\ \tilde{\mathbf{h}}_\mathbf{2} &= -\left(w_2^2\mathbf{I}+\mathbf{A}^2\right)^{-1}\mathbf{Ab}\\ \tilde{\mathbf{p}}_\mathbf{2} &= -\left(w_2^2\mathbf{I}+\mathbf{A}^2\right)^{-1}w_2\mathbf{b}.\end{aligned} \tag{24}$$

The output $y_{n\ell\ell}$ is proportional to the third Hadamard power of $\mathbf{x}$. The complete expression of $\mathbf{x}^{\bullet 3}$ is given in Appendix C. By keeping only the components of $\mathbf{x}^{\bullet 3}$ at frequencies w_1, w_2, and $2w_1 - w_2$ and multiplying from the left with $\alpha\mathbf{c}^T$, we get

$$\begin{aligned}\hat{y}_{n\ell\ell}(t) = \alpha\frac{3}{4}{k_1}^2k_2\mathbf{c}^T&(\tilde{\mathbf{s}}_{2,-1}\sin(\Omega_{\boldsymbol{I}}t)+\tilde{\mathbf{c}}_{\mathbf{2,-1}}\cos(\Omega_{\boldsymbol{I}}t))\\ &+\alpha\mathbf{c}^T(\mathbf{s_{3,0}}\sin(w_1t)+\mathbf{c_{3,0}}\cos(w_1t))\\ &+\alpha\mathbf{c}^T(\mathbf{s_{0,3}}\sin(w_2t)+\mathbf{c_{0,3}}\cos(w_2t))\end{aligned} \tag{25}$$

where

$$\begin{aligned}\tilde{\mathbf{s}}_{\mathbf{2},-\mathbf{1}} &= \tilde{\mathbf{h}}_\mathbf{1}^{\bullet 2}\bullet\tilde{\mathbf{h}}_\mathbf{2}+2\tilde{\mathbf{h}}_\mathbf{1}\bullet\tilde{\mathbf{p}}_\mathbf{1}\bullet\tilde{\mathbf{p}}_\mathbf{2}-\tilde{\mathbf{p}}_\mathbf{1}^{\bullet 2}\bullet\tilde{\mathbf{h}}_\mathbf{2}\\ \tilde{\mathbf{c}}_{\mathbf{2},-\mathbf{1}} &= \tilde{\mathbf{p}}_\mathbf{1}^{\bullet 2}\bullet\tilde{\mathbf{p}}_\mathbf{2}+2\tilde{\mathbf{h}}_\mathbf{1}\bullet\tilde{\mathbf{p}}_\mathbf{1}\bullet\tilde{\mathbf{h}}_\mathbf{2}-\tilde{\mathbf{h}}_\mathbf{1}^{\bullet 2}\bullet\tilde{\mathbf{p}}_\mathbf{2}\\ \mathbf{s_{3,0}} &= \frac{3}{4}\left(\mathbf{h_1}\bullet\mathbf{p_1^{\bullet 2}}+2\mathbf{h_1}\bullet\mathbf{h_2^{\bullet 2}}+2\mathbf{h_1}\bullet\mathbf{p_2^{\bullet 2}}+\mathbf{h_1^{\bullet 3}}\right)\\ \mathbf{c_{3,0}} &= \frac{3}{4}\left(\mathbf{h_1^{\bullet 2}}\bullet\mathbf{p_1}+\mathbf{p_1^{\bullet 3}}+2\mathbf{p_1}\bullet\mathbf{h_2^{\bullet 2}}+2\mathbf{p_1}\bullet\mathbf{p_2^{\bullet 2}}\right)\\ \mathbf{s_{0,3}} &= \frac{3}{4}\left(\mathbf{h_2}\bullet\mathbf{p_2^{\bullet 2}}+2\mathbf{p_1^{\bullet 2}}\bullet\mathbf{h_2}+\mathbf{h_2^{\bullet 3}}+2\mathbf{h_1^{\bullet 2}}\bullet\mathbf{h_2}\right)\\ \mathbf{c_{0,3}} &= \frac{3}{4}\left(\mathbf{h_2^{\bullet 2}}\bullet\mathbf{p_2}+\mathbf{p_2^{\bullet 3}}+2\mathbf{p_1^{\bullet 2}}\bullet\mathbf{p_2}+2\mathbf{h_1^{\bullet 2}}\bullet\mathbf{p_2}\right).\end{aligned} \tag{26}$$

Column vectors $\tilde{\mathbf{s}}_{\mathbf{2},-\mathbf{1}}$ and $\tilde{\mathbf{c}}_{\mathbf{2},-\mathbf{1}}$ are independent of the amplitudes k_1 and k_2. Column vectors $\mathbf{s_{3,0}}, \mathbf{c_{3,0}}, \mathbf{s_{0,3}}$, and $\mathbf{c_{0,3}}$ are third-order homogeneous functions of (k_1, k_2).

D. Nonlinear Filter Core: Operator $S_3^\ell \circ S_2^n \circ S_1^\ell$

The nonlinearity of the core is captured by the third term, $S_3^\ell \circ S_2^n \circ S_1^\ell$, in expression (15) corresponding to the block diagram of Fig. 9. Derivation of the IMD is more involved here (versus input, output stages) since we have a dynamical system with nonlinear feedback path.

By definition, $S_3^\ell \circ S_2^n \circ S_1^\ell$, is the deviation of the filter core's behavior from that of the ideal (linear) one. This deviation is a "small" perturbation of the linear system and is treated in the following subsection using *regular perturbation theory* [20]–[22].

1) Modelling Weakly Nonlinear Behavior Using Regular Perturbation Theory: The dynamics of the weakly nonlinear core is modeled by the system of differential equations

$$\dot{\mathbf{x}}(t) = \mathbf{Ax}(t)+\alpha\mathbf{Ax}^{\bullet 3}(t)+\mathbf{b}u(t) \tag{27}$$

where α is the small ($|\alpha| \ll 1$) nonlinearity parameter of the transconductors.[6] Following [21], the solution of (27) can be written as an infinite power series on α, i.e.,

$$\mathbf{x}(t) = \mathbf{x_0}(t)+\alpha\mathbf{x_1}(t)+\alpha^2\mathbf{x_2}(t)+\alpha^3\mathbf{x_3}(t)+\cdots. \tag{28}$$

Replacing (28) into (27), we get

$$\begin{aligned}\dot{\mathbf{x}}_0+\alpha\dot{\mathbf{x}}_1+\alpha^2\dot{\mathbf{x}}_2+\cdots &= \mathbf{A}(\mathbf{x_0}+\alpha\mathbf{x_1}+\alpha^2\mathbf{x_2}+\cdots)\\ &\quad+\alpha\mathbf{A}(\mathbf{x_0}+\alpha\mathbf{x_1}+\alpha^2\mathbf{x_2}\ldots)^{\bullet 3}+\mathbf{b}u.\end{aligned}$$

Expanding $\mathbf{x}^{\bullet 3}$ and grouping terms according to the power of α gives

$$\begin{aligned}(\mathbf{x_0}+\alpha\mathbf{x_1}+\alpha^2\mathbf{x_2}+\cdots)^{\bullet 3} &= \mathbf{x_0}^{\bullet 3}+3\alpha\mathbf{x_1}\bullet\mathbf{x_0}^{\bullet 2}\\ &\quad+3\alpha^2(\mathbf{x_2}\bullet\mathbf{x_0}^{\bullet 2}+\mathbf{x_1}^{\bullet 2}\bullet\mathbf{x_0})+\cdots.\end{aligned}$$

Combining the last two equations and grouping the terms based on the power of α results in

$$\begin{aligned}\dot{\mathbf{x}}_0+\alpha\dot{\mathbf{x}}_1+\alpha^2\dot{\mathbf{x}}_2+\cdots &= \mathbf{Ax_0}+\mathbf{b}u+\alpha\mathbf{A}(\mathbf{x_1}+\mathbf{x_0}^{\bullet 3})\\ &\quad+\alpha^2\mathbf{A}(\mathbf{x_2}+3\mathbf{x_1}\bullet\mathbf{x_0^{\bullet 2}})+\cdots.\end{aligned} \tag{29}$$

The solution of (29) can be derived by solving the following (infinite) set of differential equations resulting from (29) by equating left and right terms based on the power of α, i.e.,

$$\dot{\mathbf{x}}_0 = \mathbf{Ax_0}+\mathbf{b}u \tag{30}$$
$$\dot{\mathbf{x}}_1 = \mathbf{Ax_1}+\mathbf{Ax_0}^{\bullet 3} \tag{31}$$
$$\dot{\mathbf{x}}_2 = \mathbf{Ax_2}+3\mathbf{A}(\mathbf{x_1}\bullet\mathbf{x_0^{\bullet 2}}) \tag{32}$$
$$\vdots$$

In principle, this infinite set of differential equations can be solved sequentially providing the exact $\mathbf{x}$. However, since α is assumed small and all distortion components are also expected to be small relatively to the desirable signals at frequencies w_1 and $w_2, \mathbf{x}$ can be approximated by only the first two term in series (28), i.e., $\mathbf{x} \approx \mathbf{x_0}+\alpha\mathbf{x_1}$.

Note that (30) models the linear filter (the top equation (21)) and so $\mathbf{x_0}$ is given by (33) with $\mathbf{h_1}, \mathbf{p_1}, \mathbf{h_2}$, and $\mathbf{p_2}$ given by (23).

$$\begin{aligned}\mathbf{x_0}(t) = \mathbf{h_1}&\sin(w_1t)+\mathbf{p_1}\cos(w_1t)\\ &+\mathbf{h_2}\sin(w_2t)+\mathbf{p_2}\cos(w_2t).\end{aligned} \tag{33}$$

The third Hadamard power of $\mathbf{x_0}$ needed to solve (31) is given by (62) in Appendix C. Moreover, (31) is linear in $\mathbf{x_0}^{\bullet 3}$ and so only the components of $\mathbf{x_0}^{\bullet 3}$ at frequencies w_1, w_2, and $2w_1 - w_2$ are required since they generate the

[6]See also Appendix A.

corresponding ones of $\mathbf{x_1}$. By taking advantage of the calculations done in Section III-C, we get (34) where constants $\mathbf{s_{2,-1}}, \mathbf{c_{2,-1}}, \mathbf{s_{3,0}}, \mathbf{c_{3,0}}, \mathbf{s_{0,3}}$ and $\mathbf{c_{0,3}}$ are given by (26)

$$\begin{aligned}\widehat{\mathbf{x_0}^{\bullet 3}}(t) &= \frac{3}{4}{k_1}^2 k_2 (\tilde{\mathbf{s}}_{\mathbf{2,-1}} \sin(\Omega_{\boldsymbol{I}} t) + \tilde{\mathbf{c}}_{\mathbf{2,-1}} \cos(\Omega_{\boldsymbol{I}} t)) \\ &\quad + \mathbf{s_{3,0}} \sin(w_1 t) + \mathbf{c_{3,0}} \cos(w_1 t) \\ &\quad + \mathbf{s_{0,3}} \sin(w_2 t) + \mathbf{c_{0,3}} \cos(w_2 t). \end{aligned} \tag{34}$$

Using the derivation in Appendix B it is concluded that

$$\begin{aligned}\hat{\mathbf{x}}_1(t) = &-\frac{3}{4}{k_1}^2 k_2 \left(\Omega_{\boldsymbol{I}}^2 \mathbf{I} + \mathbf{A}^2\right)^{-1} \\ &\times (\mathbf{A}^2 \tilde{\mathbf{s}}_{\mathbf{2,-1}} - \Omega_{\boldsymbol{I}} \mathbf{A} \tilde{\mathbf{c}}_{\mathbf{2,-1}}) \sin(\Omega_{\boldsymbol{I}} t) \\ &- \frac{3}{4}{k_1}^2 k_2 \left(\Omega_{\boldsymbol{I}}^2 \mathbf{I} + \mathbf{A}^2\right)^{-1} \\ &\times \left(\mathbf{A}^2 \tilde{\mathbf{c}}_{\mathbf{2,-1}} + \Omega_{\boldsymbol{I}} \mathbf{A} \tilde{\mathbf{s}}_{\mathbf{2,-1}}\right) \cos(\Omega_{\boldsymbol{I}} t) \\ &- \left(w_1^2 \mathbf{I} + \mathbf{A}^2\right)^{-1} \left(\mathbf{A}^2 \mathbf{s_{3,0}} - w_1 \mathbf{A} \mathbf{c_{3,0}}\right) \sin(w_1 t) \\ &- \left(w_1^2 \mathbf{I} + \mathbf{A}^2\right)^{-1} \left(\mathbf{A}^2 \mathbf{c_{3,0}} + w_1 \mathbf{A} \mathbf{s_{3,0}}\right) \cos(w_1 t) \\ &- \left(w_2^2 \mathbf{I} + \mathbf{A}^2\right)^{-1} \left(\mathbf{A}^2 \mathbf{s_{0,3}} - w_2 \mathbf{A} \mathbf{c_{0,3}}\right) \sin(w_2 t) \\ &- \left(w_2^2 \mathbf{I} + \mathbf{A}^2\right)^{-1} \left(\mathbf{A}^2 \mathbf{c_{0,3}} + w_2 \mathbf{A} \mathbf{s_{0,3}}\right) \cos(w_2 t). \end{aligned}$$

From Fig. 9, we get $y_{\ell n \ell}(t) = \alpha \mathbf{c}^T \mathbf{x_1}(t) + \alpha^2 \mathbf{c}^T \mathbf{x_2}(t) + \alpha^3 \mathbf{c}^T \mathbf{x_3}(t) + \cdots$ which reduces to $y_{\ell n \ell}(t) \approx \alpha \mathbf{c}^T \mathbf{x_1}(t)$ following the approximation $\mathbf{x} \approx \mathbf{x_0} + \alpha \mathbf{x_1}$. Therefore, it is

$$\hat{y}_{\ell n \ell}(t) \approxeq \alpha \mathbf{c}^T \hat{\mathbf{x}}_1(t). \tag{35}$$

E. Total IMD

The total response of the weakly nonlinear filter is approximated[7] by the superposition of the four signal paths analyzed in Sections III-A–III-D. Therefore,

$$\begin{aligned} y(t) &\approxeq \left(S_3^\ell \circ S_2^\ell \circ S_1^\ell\right)(u) + \left(S_3^\ell \circ S_2^\ell \circ S_1^n\right)(u) \\ &\quad + \left(S_3^\ell \circ S_2^n \circ S_1^\ell\right)(u) + \left(S_3^n \circ S_2^\ell \circ S_1^\ell\right)(u) \\ &= y_{\ell\ell\ell}(t) + y_{\ell\ell n}(t) + y_{\ell n \ell}(t) + y_{n \ell\ell}(t) \end{aligned}$$

[7]. . . for IMD estimation. See the discussion leading to expression (15).

which implies $\hat{y}(t) \approxeq \hat{y}_{\ell\ell\ell}(t) + \hat{y}_{\ell\ell n}(t) + \hat{y}_{\ell n \ell}(t) + \hat{y}_{n\ell\ell}(t)$ whose summands are given by (18), (20), (35) and (25). Specifically, the total component at the output at frequency $\Omega_{\boldsymbol{I}} = 2w_1 - w_2$

$$\hat{y}_{\Omega_{\boldsymbol{I}}} \approxeq \hat{y}_{\ell\ell n}|_{\Omega_{\boldsymbol{I}}} + \hat{y}_{\ell n \ell}|_{\Omega_{\boldsymbol{I}}} + \hat{y}_{n \ell\ell}|_{\Omega_{\boldsymbol{I}}}$$

is given by (36) [using (20), (35), and (25)]

$$\hat{y}_{\Omega_{\boldsymbol{I}}} \approxeq \alpha \frac{3{k_1}^2 k_2}{4} (S_{2,-1} \sin(\Omega_{\boldsymbol{I}} t) + C_{2,-1} \cos(\Omega_{\boldsymbol{I}} t)) \tag{36}$$

where

$$\begin{aligned} S_{2,-1} &= \underbrace{-\mathbf{c}^T \mathbf{F} \mathbf{A} \mathbf{b}}_{\text{input}} \underbrace{-\mathbf{c}^T \mathbf{F} (\mathbf{A}^2 \tilde{\mathbf{s}}_{\mathbf{2,-1}} - \Omega_{\boldsymbol{I}} \mathbf{A} \tilde{\mathbf{c}}_{\mathbf{2,-1}})}_{\text{filter core}} \\ &\quad + \underbrace{\mathbf{c}^T \tilde{\mathbf{s}}_{\mathbf{2,-1}}}_{\text{output}} \end{aligned} \tag{37}$$

$$\begin{aligned} C_{2,-1} &= \underbrace{-\Omega_{\boldsymbol{I}} \mathbf{c}^T \mathbf{F} \mathbf{b}}_{\text{input}} \underbrace{-\mathbf{c}^T \mathbf{F} (\mathbf{A}^2 \tilde{\mathbf{c}}_{\mathbf{2,-1}} + \Omega_{\boldsymbol{I}} \mathbf{A} \tilde{\mathbf{s}}_{\mathbf{2,-1}})}_{\text{filter core}} \\ &\quad + \underbrace{\mathbf{c}^T \tilde{\mathbf{c}}_{\mathbf{2,-1}}}_{\text{output}} \end{aligned} \tag{38}$$

and $\mathbf{F} \triangleq (\Omega_{\boldsymbol{I}}^2 \mathbf{I} + \mathbf{A}^2)^{-1}$.

It is worth mentioning that **$\mathbf{S_{2,-1}}$ and $\mathbf{C_{2,-1}}$ are independent of k_1 and k_2**. Also, expressions (37) and (38) are the sums of the frequency components at $\Omega_{\boldsymbol{I}} = 2w_1 - w_2$ introduced by the input, the filter core and the output stages divided by the factor $\alpha 3{k_1}^2 k_2/4$. *If a stage is linear, or, it does not exist (e.g., the output may be a state variable x_i), the corresponding terms in* (37), (38) *must be removed*. Finally, the amplitude of $\hat{y}_{\Omega_{\boldsymbol{I}}}$ is

$$\mathcal{A}_{\Omega_{\boldsymbol{I}}} \approxeq |\alpha| \frac{3{k_1}^2 k_2}{4} \sqrt{(S_{2,-1})^2 + (C_{2,-1})^2}. \tag{39}$$

The total component at the output at frequency w_1 (similarly for w_2) is shown in (40), at the bottom of the page.

The component at w_1 is dominated by the response of the linear (ideal) filter $y_{\ell\ell\ell}$. This approximation is used in the calculation of IM_3. The rest of the terms in (40) are used to estimate

$$\begin{aligned} \hat{y}_{w_1}(t) &\approxeq \hat{y}_{\ell\ell\ell}(t)|_{w_1} + \hat{y}_{\ell\ell n}(t)|_{w_1} + \hat{y}_{\ell n \ell}(t)|_{w_1} + \hat{y}_{n\ell\ell}(t)|_{w_1} \\ &= \left.\begin{aligned} &-k_1 \mathbf{c}^T \left(w_1^2 \mathbf{I} + \mathbf{A}^2\right)^{-1} \mathbf{A} \mathbf{b} \sin(w_1 t) \\ &-k_1 \mathbf{c}^T \left(w_1^2 \mathbf{I} + \mathbf{A}^2\right)^{-1} w_1 \mathbf{b} \cos(w_1 t) \end{aligned}\right\} \text{Linear path} \\ &\quad \left.\begin{aligned} &-\alpha \left(\tfrac{3}{2} k_1 {k_2}^2 + \tfrac{3}{4} {k_1}^3\right) \mathbf{c}^T ({w_1}^2 \mathbf{I} + \mathbf{A}^2)^{-1} \mathbf{A} \mathbf{b} \sin(w_1 t) \\ &-\alpha \left(\tfrac{3}{2} k_1 {k_2}^2 + \tfrac{3}{4} {k_1}^3\right) \mathbf{c}^T ({w_1}^2 \mathbf{I} + \mathbf{A}^2)^{-1} w_1 \mathbf{b} \cos(w_1 t) \end{aligned}\right\} \text{Input} \\ &\quad \left.\begin{aligned} &-\alpha \mathbf{c}^T \left(w_1^2 \mathbf{I} + \mathbf{A}^2\right)^{-1} \left(\mathbf{A}^2 \mathbf{s_{3,0}} - w_1 \mathbf{A} \mathbf{c_{3,0}}\right) \sin(w_1 t) \\ &-\alpha \mathbf{c}^T \left(w_1^2 \mathbf{I} + \mathbf{A}^2\right)^{-1} \left(\mathbf{A}^2 \mathbf{c_{3,0}} + w_1 \mathbf{A} \mathbf{s_{3,0}}\right) \cos(w_1 t) \end{aligned}\right\} \text{Core} \\ &\quad \left.\begin{aligned} &+\alpha \mathbf{c}^T \mathbf{s_{3,0}} \sin(w_1 t) \\ &+\alpha \mathbf{c}^T \mathbf{c_{3,0}} \cos(w_1 t) \end{aligned}\right\} \text{Output} \end{aligned} \tag{40}$$

the relative error in IM_3 calculation using the proposed method. Therefore

$$\hat{y}_{w_1}(t) \approxeq -k_1\mathbf{c}^T\left(w_1^2\mathbf{I}+\mathbf{A}^2\right)^{-1}w_1\mathbf{b}\cos(w_1 t) - k_1\mathbf{c}^T\left(w_1^2\mathbf{I}+\mathbf{A}^2\right)^{-1}\mathbf{A}\mathbf{b}\sin(w_1 t) \quad (41)$$

with amplitude shown in (42), at the bottom of the page.[8]

The part of $\hat{y}_{w_1}$ (40) resulting from the filter's weak nonlinearities is

$$\hat{y}_{w_1}^{\alpha}(t) = S_{1,0}^{\alpha}\sin(w_1 t) + C_{1,0}^{\alpha}\cos(w_1 t)$$

where

$$S_{1,0}^{\alpha} = -\alpha\mathbf{c}^T\left(({w_1}^2\mathbf{I}+\mathbf{A}^2)^{-1}\mathbf{A}\left(\kappa\mathbf{b}+\mathbf{A}\mathbf{s_{3,0}}-w_1\mathbf{c_{3,0}}\right)-\mathbf{s_{3,0}}\right)$$
$$C_{1,0}^{\alpha} = -\alpha\mathbf{c}^T\left(({w_1}^2\mathbf{I}+\mathbf{A}^2)^{-1}\mathbf{A}(\kappa w_1\mathbf{b}+\mathbf{A}\mathbf{c_{3,0}}+w_1\mathbf{s_{3,0}})-\mathbf{c_{3,0}}\right) \quad (43)$$

and $\kappa = (3/2)k_1{k_2}^2 + (3/4){k_1}^3$.

The amplitude $\mathcal{A}_{w_1}^{\alpha}$ of $\hat{y}_{w_1}^{\alpha}$, given by (44), is typically negligible with respect to $\mathcal{A}_{w_1}$. The ratio $\mathcal{A}_{w_1}^{\alpha}/\mathcal{A}_{w_1}$ is used later in this section as an indicator of the percentile error of the IM_3 estimate

$$\mathcal{A}_{w_1}^{\alpha} = \sqrt{\left(S_{1,0}^{\alpha}\right)^2 + \left(C_{1,0}^{\alpha}\right)^2}. \quad (44)$$

Signal component $\hat{y}_{w_2}$ and the corresponding amplitude $\mathcal{A}_{w_2}$ are derived from (40)–(44) simply by interchanging k_1 with k_2 and w_1 with w_2.

Finally, the standard definition of the *third-order IMD referred to input component at* w_1, [16], [17], $\mathrm{IM}_3 \triangleq \mathcal{A}_{\Omega_I}/\mathcal{A}_{w_1}$, and expressions (39), (42) we give

$$\mathrm{IM}_3 \approxeq |\alpha|\frac{3k_1k_2}{4}\mathcal{J}(w_1,w_2) \quad (45)$$

where $\mathcal{J}$ is given by (46), shown at the bottom of the page.

Note that $\mathcal{J}(w_1,w_2)$ depends *only* on ideal filter's parameters, i.e., matrices $\mathbf{A}, \mathbf{b}$, and $\mathbf{c}$, and frequencies w_1 and w_2; *it is independent of the amplitudes* k_1 *and* k_2.

It is worth comparing (45) to the IM_3 introduced by a *static* weakly nonlinear function of the form $v = f(u) = a_1u + a_2u^2 + a_3u^3 + \cdots$ where $u = k_1\sin(w_1t) + k_2\sin(w_2t)$. In the static case, the IM_3 referred to input component at w_1, is $\mathrm{IM}_3^{\mathrm{static}} = |a_3/a_1|(3k_1k_2/4)$, (e.g., [16], [17]). Note first that in the *I-V* characteristic of the transconductors, expression (2), α equals a_3/a_1. Moreover, it can be verified from (46) that $\mathcal{J}(w_1,w_2) \to 1$ when $w_1, w_2 \to 0$. *Therefore, in the low-frequency regime*, IM_3 *derived in this work equals* $\mathrm{IM}_3^{\mathrm{static}}$.

[8]Note that $\sqrt{{w_1}^2(\mathbf{c}^T(w_1^2\mathbf{I}+\mathbf{A}^2)^{-1}\mathbf{b})^2 + (\mathbf{c}^T(w_1^2\mathbf{I}+\mathbf{A}^2)^{-1}\mathbf{A}\mathbf{b})^2} = |\mathbf{c}^T(jw_1\mathbf{I}-\mathbf{A})^{-1}\mathbf{b}|$, because $\hat{y}_{w_1}(t)$ is the response of the linear filter with transfer function $\mathbf{c}^T(jw\mathbf{I}-\mathbf{A})^{-1}\mathbf{b}$ at frequency $w = w_1$.

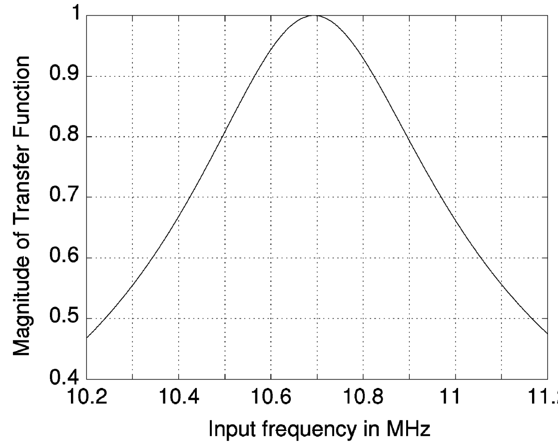

Fig. 10. Magnitude of the transfer function in linear scale.

To illustrate the role of function $\mathcal{J}(w_1,w_2)$ lets consider the weakly nonlinear filter in Fig. 2 (and Fig. 14, shown later) with parameters given by (47). It is a Tow–Thomas bandpass biquad, centered at 10.7 MHz, [4] and it is discussed in detail in Section IV

$$\mathbf{A} = 10^6\begin{bmatrix}-3.36 & -67.2\\ 67.2 & 0\end{bmatrix}$$
$$\mathbf{b} = 10^6\begin{bmatrix}3.36\\ 0\end{bmatrix}$$
$$\mathbf{c} = [1, \quad 0]^T$$
$$\alpha = -0.0535. \quad (47)$$

The amplitude of the transfer function of the filter is shown in Fig. 10 and function $\mathcal{J}(w_1,w_2)$ is shown in Fig. 11. Comparing the figures and using (45) it is concluded that distortion is approximately maximized when the input frequencies w_1, w_2 coincide with the peak frequency of the bandpass filter.

A rough estimate of the error in the evaluation of IM_3 is given by the ratio $\mathcal{A}_{w_1}^{\alpha}/\mathcal{A}_{w_1}$. The rationale is that $\mathcal{A}_{w_1}$ is the zeroth-order approximation of the amplitude at w_1 with respect

$$\mathcal{A}_{w_1} \approxeq k_1\sqrt{{w_1}^2\left(\mathbf{c}^T\left(w_1^2\mathbf{I}+\mathbf{A}^2\right)^{-1}\mathbf{b}\right)^2 + \left(\mathbf{c}^T\left(w_1^2\mathbf{I}+\mathbf{A}^2\right)^{-1}\mathbf{A}\mathbf{b}\right)^2} \quad (42)$$

$$\mathcal{J}(w_1,w_2) = \sqrt{\frac{(S_{2,-1})^2+(C_{2,-1})^2}{{w_1}^2\left(\mathbf{c}^T\left(w_1^2\mathbf{I}+\mathbf{A}^2\right)^{-1}\mathbf{b}\right)^2 + \left(\mathbf{c}^T\left(w_1^2\mathbf{I}+\mathbf{A}^2\right)^{-1}\mathbf{A}\mathbf{b}\right)^2}} \quad (46)$$

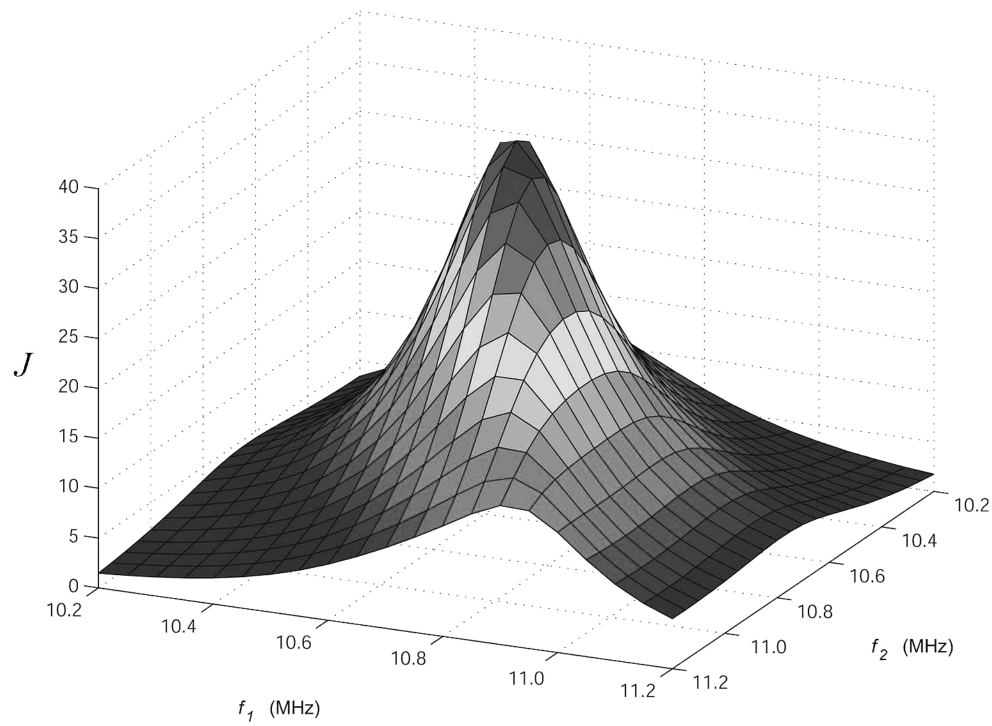

Fig. 11. $J(2\pi f_1, 2\pi f_2)$ in linear scale.

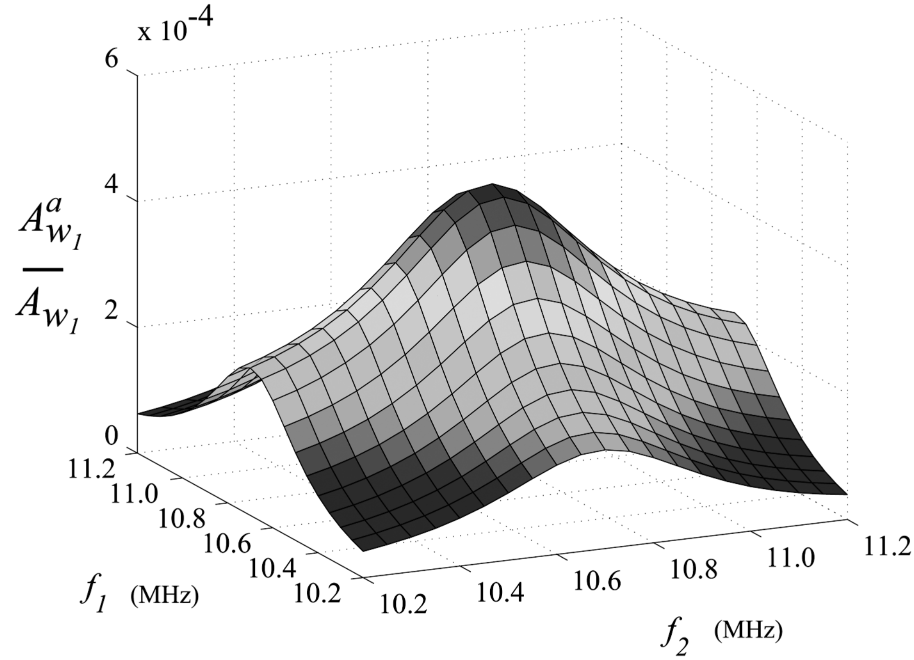

Fig. 12. $\mathcal{A}^{\alpha}_{w_1}/\mathcal{A}_{w_1}$ as a function of f_1, f_2 with $k_1 = k_2 = 0.01$ V.

to nonlinearity parameter α, while $\mathcal{A}^{\alpha}_{w_1}$ represents the size of the components at w_1 linearly depending on α. The ratio is shown in Figs. 12 and 13 as a function of w_1, w_2, when $k_1 = k_2 = 0.01$ V and $k_1 = k_2 = 0.1$ V, respectively.

IV. SPICE AND MATLAB SIMULATION

Two filters were designed in a standard CMOS 0.5-μm process using Cadence. SpectreS (SPICE) and Simulink (MATLAB) simulation was performed to verify the proposed methodology. The experimental setup is introduced in Sections IV-A and IV-B and the results are discussed in detail in Section IV-C.

A. Test Circuit 1: Tow–Thomas Bandpass Filter

The first test filter is the fully differential, second-order Tow–Thomas bandpass in Fig. 14. The filter's input is $u(t) = k_1 \sin(w_1 t) + k_2 \sin(w_2 t)$ and the state variables are the differential voltages $x_1 = X_{1+} - X_{1-}$ and $x_2 = X_{2+} - X_{2-}$. The output is $y = x_2$ and so *there is no output stage* as in

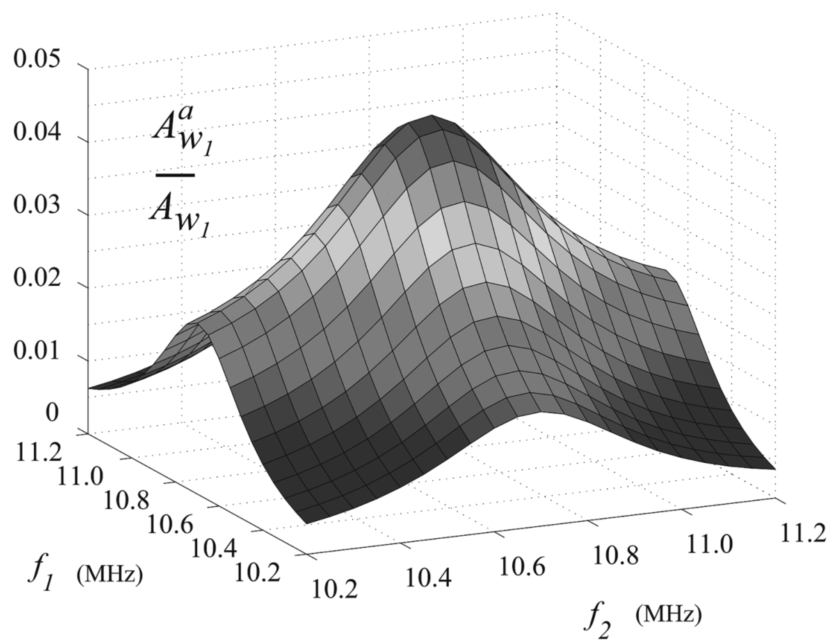

Fig. 13. $\mathcal{A}^{\alpha}_{w_1}/\mathcal{A}_{w_1}$ as a function of f_1, f_2 with $k_1 = k_2 = 0.1$ V.

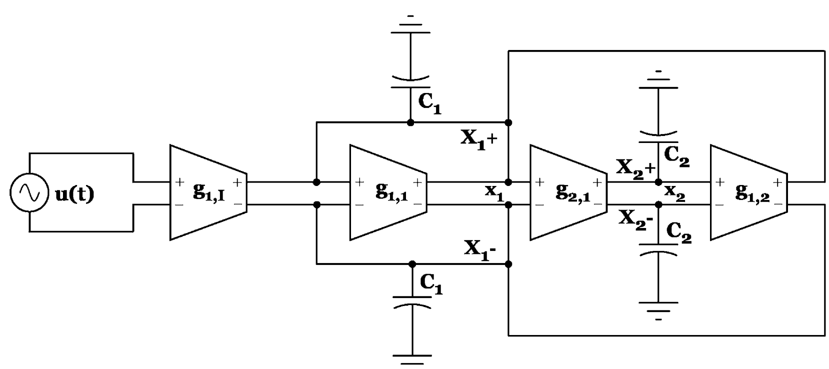

Fig. 14. Designed Tow–Thomas biquad filter.

Fig. 2. The state-space equations of the ideal (linear) filter and the corresponding structural matrices $\mathbf{A}, \mathbf{b}$, and $\mathbf{c}$ are

$$\begin{bmatrix} \dot{x}_1(t) \\ \dot{x}_2(t) \end{bmatrix} = \underbrace{\begin{bmatrix} \frac{g_{1,1}}{C_1} & \frac{g_{2,1}}{C_1} \\ \frac{g_{1,2}}{C_2} & 0 \end{bmatrix}}_{\mathbf{A}} \begin{bmatrix} x_1(t) \\ x_2(t) \end{bmatrix} + \underbrace{\begin{bmatrix} \frac{g_{1,I}}{C_1} \\ 0 \end{bmatrix}}_{\mathbf{b}} u(t) \tag{48}$$

and

$$y(t) = \underbrace{[1 \quad 0]}_{\mathbf{c}^T} \begin{bmatrix} x_1(t) \\ x_2(t) \end{bmatrix}. \tag{49}$$

The transfer function of the filter is

$$H(jw) = \frac{\frac{g_{1,I}}{C_1} s}{s^2 + \frac{g_{1,1}}{C_1} s + \frac{g_{1,2} g_{2,1}}{C_1 C_2}} \tag{50}$$

where

$$f_o = \frac{1}{2\pi} \sqrt{\frac{g_{1,2} g_{2,1}}{C_1 C_2}} \quad \text{and} \quad Q = \sqrt{\frac{C_1 g_{1,2} g_{2,1}}{C_2 g_{1,1}^2}} \tag{51}$$

The fully differential transconductor used in the filter is shown in Fig. 15. Its balanced structure suppresses even-order nonlinearities. The differential pair M_1-M_2 is primarily responsible for the (odd-order) nonlinearity of the transconductor. Common mode feedback is realized by M_{11}, M_{12} and M_{13}.

The central frequency of the second-order bandpass filter is $f_o = 10.7$ MHz and the quality factor is $Q = 20$. The values of the transconductances and capacitors are given in Table I.

Since there is no output stage, the calculation of $S_{2,-1}$ and $C_{2,-1}$ is done by ignoring the last terms in expressions (37) and (38).

Parameter α was estimated by curve-fitting: the *I–V* characteristic of the transconductor was derived from Cadence (SpectreS) simulation; a third-order polynomial was fit to it. The estimated value of α is in Table I. Analytical estimation of α is also possible (Appendix A).

B. Test Circuit 2: Fourth-Order Cascade Filter

The fourth-order bandpass filter in Fig. 16 is a cascade of two Tow–Thomas biquads identical to that in Section IV-A. Being a cascade, this filter is used to verify and demonstrate the proposed methodology, and also, to illustrate the validity of the main assumption in Section III, i.e., superposition of IMD components generated by different parts of the circuit can be used

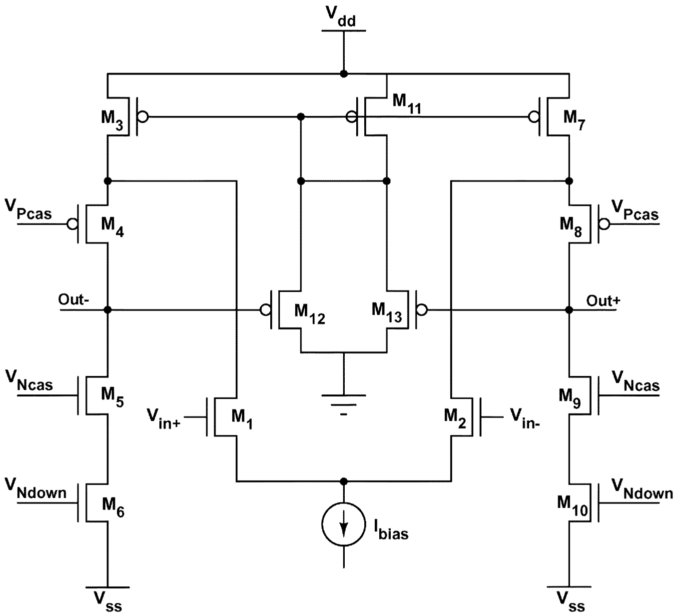

Fig. 15. Transconductor's circuit.

TABLE I
SECOND-ORDER FILTER'S PARAMETERS

Parameter	α	$g_{1,I}$	$g_{1,1}$
Value	-0.0535 V^{-2}	31.26 μA/V	-31.26 μA/V
Parameter	$g_{2,1}$	$g_{1,2}$	$C_1 = C_2$
Value	625.2 μA/V	-625.2 μA/V	9.3054 pF

as long as the circuit components are weakly nonlinear; in this case we want to verify that the estimated total IM_3 at the output is approximately equal to the sum of that of the first biquad, (linearly) propagated through the second one, plus the IM_3 of the second biquad.

The input signal is $u(t) = k_1 \sin(w_1 t) + k_2 \sin(w_2 t)$ and the state variables are the differential voltages $x_i = X_{i+} - X_{i-}$, $i = 1, 2, 3, 4$. The state-space equations of the ideal (linear) filter are

$$\begin{bmatrix} \dot{x}_1 \\ \dot{x}_2 \\ \dot{x}_3 \\ \dot{x}_4 \end{bmatrix} = \underbrace{\begin{bmatrix} \frac{g_{1,1}}{C_1} & \frac{g_{1,2}}{C_1} & 0 & 0 \\ \frac{g_{2,1}}{C_2} & 0 & 0 & 0 \\ 0 & \frac{g_{3,2}}{C_3} & \frac{g_{3,3}}{C_3} & \frac{g_{3,4}}{C_3} \\ 0 & 0 & \frac{g_{4,3}}{C_4} & 0 \end{bmatrix}}_{\mathbf{A}} \begin{bmatrix} x_1 \\ x_2 \\ x_3 \\ x_4 \end{bmatrix} + \underbrace{\begin{bmatrix} \frac{g_{1,I}}{C_1} \\ 0 \\ 0 \\ 0 \end{bmatrix}}_{\mathbf{b}} u(t) \tag{52}$$

and

$$y(t) = \underbrace{[0 \quad 0 \quad 1 \quad 0]}_{\mathbf{c}^T} \begin{bmatrix} x_1(t) \\ x_2(t) \\ x_3(t) \\ x_4(t) \end{bmatrix}. \tag{53}$$

The fully differential transconductors are identical to those used in Section IV-A and are shown in Fig. 15. The Q of the filter is 32. Again, there is no output stage and so the calculation of $S_{2,-1}$ and $C_{2,-1}$ is done by ignoring the last terms in expressions (37) and (38), respectively. The value of the nonlinear scale factor α is the same as before and is shown in Table II along with the values of the transconductances and capacitors.

TABLE II
FOURTH-ORDER FILTER'S PARAMETERS

Parameter	α	$g_{1,I}, g_{3,1}$	$g_{1,1}, g_{3,3}$
Value	-0.0535 V^{-2}	31.26 μA/V	-31.26 μA/V
Parameter	$g_{2,1}, g_{4,3}$	$g_{1,2}, g_{3,4}$	C_1, C_2, C_3, C_4
Value	625.2μA/V	-625.2μA/V	9.3054 pF

C. Simulation Results

Two sets of experiments were performed on both filters: SpectreS (SPICE) simulation, using bsim3v3 transistor models [24], and Simulink6 © simulation of the weakly nonlinear state-space models of the filters. Comparison between SpectreS and theory provides an estimate of the error in IMD calculation that is due to: simplifications and assumptions needed to extract the (weakly nonlinear) state-space model of the filter as well as all mathematical approximations. Comparison between Simulink and theory provides an estimate of the IMD calculation error due to: the approximate solution of the nonlinear system of differential equations using the perturbation technique (here the third-order IMD components generated by higher perturbation terms are omitted).

1) Tow–Thomas Bandpass Filter: Two tests were performed on the second-order filter: 1) The filter was driven by $u(t) = k_1 \sin(2\pi f_1 t) + k_2 \sin(2\pi f_2 t)$ with $k_1 = k_2 = 1$ mV, 10 mV and 100 mV, using three pairs of frequencies f_1, f_2 around the central frequency of 10.7 MHz. The amplitudes of the output signal components at frequencies f_1, f_2 and $2f_1 - f_2$, estimated using SpectreS simulation, Simulink and the proposed theory are shown in Table III. The *error* values are the differences between SpectreS and theory. All amplitudes are expressed as $20\log_{10}$ (Amplitude in Volts). 2) The filter was driven by $u(t) = k_1 \sin(2\pi f_1 t) + k_2 \sin(2\pi f_2 t)$ with $f_1 = 10.7$ MHz, $f_2 = 10.8$ MHz using three different pairs of amplitudes k_1, k_2. The results are shown in Table IV.

2) Fourth-Order Cascade Filter: The fourth-order cascade filter was simulated with input signal $u(t) = k_1 \sin(2\pi f_1 t) + k_2 \sin(2\pi f_2 t)$ with $k_1 = k_2 = 1$ mV, 10 mV, 100 mV and $f_1 = 10.7$ MHz, $f_2 = 10.8$ MHz. The amplitudes of the output signal components at frequencies f_1, f_2 and $2f_1 - f_2$, estimated using SpectreS simulation, Simulink and the proposed theory and are shown in Table V. As before, the *error* values are the differences between SpectreS and theory.

3) Comments: In all cases the theoretical results are very close to those from SpectreS and Simulink simulation. The largest errors appeared using the smallest input amplitudes in which cases the intermodulation signal at $2f_1 - f_2$ is about 110 dB below the referenced input at f_1 and therefore negligible for most applications. Finally, the IM_3 of the cascade is indeed very close to two times (6 dB) that of the second-order filter as expected since all three frequencies $2f_1, f_2$ and $2f_1 - f_2$ are very close to the central frequency of the filters corresponding to unity gain.

V. CONCLUSION

The IMD of G_m–C filters with fully balanced weakly nonlinear transconductors was derived using state-space modeling

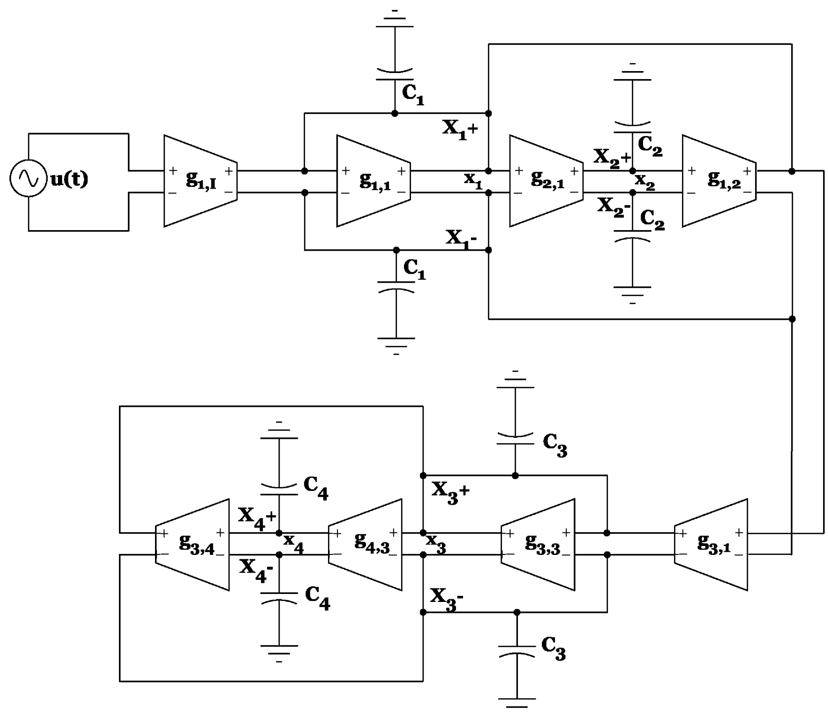

Fig. 16. Designed fourth-order bandpass filter.

TABLE III
SIMULATION RESULTS OF THE SECOND-ORDER FILTER WITH $k_1 = k_2 = 1$, 10, AND 100 mV, AND THREE PAIRS OF FREQUENCIES f_1, f_2. THE ERRORS ARE THE DIFFERENCES BETWEEN THEORETICAL AND SPECTRES SIMULATION'S RESULTS. AMPLITUDES ARE EXPRESSED AS $20\log_{10}$ (AMPLITUDE IN VOLTS)

		Frequency Pair-1			Frequency Pair-2			Frequency Pair-3		
Amplitude of the input beats		f_1	f_2	$2f_1 - f_2$	f_1	f_2	$2f_1 - f_2$	f_1	f_2	$2f_1 - f_2$
	MHz	10.6	10.5	10.7	10.6	10.8	10.4	10.7	10.8	10.6
k_1=100mV k_2=100mV	Simulink(dB)	-20.41	-21.69	-58.19	-20.40	-20.77	-60.90	-20.02	-20.779	-57.27
	Theory(dB)	-20.50	-21.85	-58.59	-20.50	-20.63	-61.35	-20.00	-20.64	-57.20
	Cadence(dB)	-19.57	-20.97	-56.82	-19.56	-20.26	-59.96	-19.25	-20.27	-56.38
	Error(dB)	0.93	0.88	1.77	0.94	0.37	1.39	0.75	0.37	0.82
k_1=10mV k_2=10mV	Simulink(dB)	-40.50	-41.85	-118.60	-40.50	-40.64	-121.10	-40.00	-40.64	-117.12
	Theory(dB)	-40.50	-41.85	-118.59	-40.50	-40.64	-121.35	-40.00	-40.64	-117.20
	Cadence(dB)	-39.64	-41.14	-116.20	-39.64	-40.11	-119.12	-39.20	-40.11	-114.97
	Error(dB)	0.86	0.71	2.39	0.86	0.53	2.23	0.80	0.54	2.23
k_1=1mV k_2=1mV	Simulink(dB)	-60.50	-61.85	-178.60	-60.50	-60.64	-181.10	-60.00	-60.64	-177.11
	Theory(dB)	-60.50	-61.85	-178.60	-60.50	-60.64	-181.35	-60.00	-60.64	-177.20
	Cadence(dB)	-59.64	-61.14	-176.43	-59.64	-60.10	-179.31	-59.20	-60.10	-175.07
	Error(dB)	0.86	0.71	2.17	0.86	0.54	2.04	0.80	0.54	2.13

and mathematical techniques based on systems and perturbation theory. The presented method results in low complexity analytic algebraic expressions that are valid for filters of any order and depend explicitly on the structural matrices of them. These properties make the proposed method a candidate for IMD estimation in optimization tools for G_m–C filters where iterations of the design are evaluated for IMD, noise, power, area and other specifications.

To verify the theory, a second- and a fourth-order G_m–C filters with fully balanced weakly nonlinear transconductors were designed, in a 0.5-μm standard CMOS process, using Cadence and were simulated in SpectreS. They were also modeled and simulated in Simulink. The IMD derived using the proposed theory was found in good agreement to that extracted from SpectreS and Simulink simulation results.

APPENDIX A

To derive the nonlinearity parameter "α" of a transconductor's *I–V* characteristic, modeled by (2), we can either: extract the *I–V* characteristic using simulation and fit a third-order polynomial to it; or, derive the analytic *I–V* expression and use Taylor expansion. The second approach is demonstrated here for the case of the transconductor in Fig. 17.

By setting $V_{\rm in} = V_{\rm in+} - V_{\rm in-}, I_{\rm out} = I_{\rm out+} - I_{\rm out-}$ and $\beta = \mu_n C_{ox} W/(2L)$, and using MOSFET's aproximate equation $i_D = \beta(v_{GS} - v_{th})^2$ it can be shown that

$$I_{\rm out} = \sqrt{2\beta I_o} \cdot V_{\rm in} \cdot \sqrt{1 - \frac{\beta V_{\rm in}^2}{2I_o}}. \quad (54)$$

TABLE IV
SIMULATION RESULTS OF THE SECOND-ORDER FILTER WITH $f_1 = 10.7$ MHZ, $f_2 = 10.8$ MHZ AND THREE PAIRS OF DIFFERENT AMPLITUDES k_1, k_2. THE ERRORS ARE THE DIFFERENCES BETWEEN THEORETICAL AND SPECTRES SIMULATION'S RESULTS. AMPLITUDES ARE EXPRESSED AS $20\log_{10}$ (AMPLITUDE IN VOLTS)

Amplitude of the input beats		f_1	f_2	$2f_1 - f_2$
	MHz	10.7	10.8	10.6
k_1=10mV k_2=100mV	Simulink	-40.01	-20.68	-97.23
	Theory(dB)	-40.01	-20.64	-97.20
	Cadence(dB)	-39.21	-20.13	-96.52
	Error(dB)	0.80	0.51	0.68
k_1=10mV k_2=10mV	Simulink	-40.00	-40.64	-117.12
	Theory(dB)	-40.00	-40.64	-117.20
	Cadence(dB)	-39.20	-40.11	-114.97
	Error(dB)	0.80	0.53	2.23
k_1=10mV k_2=1mV	Simulink	-40.00	-60.64	-137.12
	Theory(dB)	-40.00	-60.64	-137.20
	Cadence(dB)	-39.20	-60.11	-134.94
	Error(dB)	0.80	0.53	2.26

TABLE V
SIMULATION RESULTS OF FOURTH-ORDER FILTER. THE ERRORS ARE THE DIFFERENCES BETWEEN THEORETICAL AND SPECTRES SIMULATION'S RESULTS. AMPLITUDES ARE EXPRESSED AS $20\log_{10}$ (AMPLITUDE IN VOLTS)

Amplitude of the input beats		f_1	f_2	$2f_1 - f_2$
	MHz	10.7	10.8	10.6
k_1=100mV k_2=100mV	Simulink(dB)	-20.05	-21.55	-51.87
	Theory(dB)	-20.02	-21.65	-51.76
	Cadence(dB)	-18.39	-20.23	-48.06
	Error(dB)	-1.63	-1.42	-3.70
k_1=10mV k_2=10mV	Simulink(dB)	-40.01	-41.28	-111.68
	Theory(dB)	-40.01	-41.37	-111.76
	Cadence(dB)	-38.30	-39.83	-107.70
	Error(dB)	-1.71	-1.54	-4.06
k_1=1mV k_2=1mV	Simulink(dB)	-60.01	-61.28	-171.66
	Theory(dB)	-60.01	-61.36	-171.76
	Cadence(dB)	-58.30	-59.82	-167.69
	Error(dB)	-1.71	-1.54	-4.07

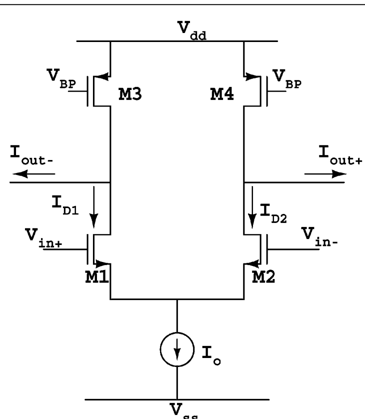

Fig. 17. Basic transconductor amplifier.

Using the Taylor expansion $\sqrt{1-x} = 1 - \frac{x}{2} + \cdots$, expression (54) gives

$$I_{\text{out}} \simeq \sqrt{2\beta I_o} V_{\text{in}} - \frac{\beta}{4I_o}\sqrt{2\beta I_o} V_{\text{in}}^3. \tag{55}$$

By comparing (55) to the model (2) we conclude that $g = \sqrt{2\beta I_o}$ and $\alpha = -\beta/(4I_o)$.

APPENDIX B

The complete solution of the dynamical system

$$\dot{\mathbf{z}}(t) = \mathbf{A}\mathbf{z}(t) + \boldsymbol{\eta}\sin(wt) + \boldsymbol{\rho}\cos(wt) \tag{56}$$

is [23]

$$\begin{aligned}\mathbf{z}(t) &= e^{\mathbf{A}t}\mathbf{z}(0) + \int_0^t e^{\mathbf{A}(t-\tau)}(\boldsymbol{\eta}\sin(w\tau) + \boldsymbol{\rho}\cos(w\tau))\,d\tau \\ &= -(\mathbf{A}^2 + w^2\mathbf{I})^{-1}(\mathbf{I}w\cos(wt) + \mathbf{A}\sin(wt) - we^{\mathbf{A}t})\boldsymbol{\eta} \\ &\quad - (\mathbf{A}^2 + w^2\mathbf{I})^{-1}(\mathbf{A}\cos(wt) - \mathbf{I}w\sin(wt) - \mathbf{A}e^{\mathbf{A}t})\boldsymbol{\rho} \\ &\quad + e^{\mathbf{A}t}\mathbf{z}(0).\end{aligned}$$

By assumption, the dynamical system is asymptotically stable (i.e., matrix $\mathbf{A}$ is Hurwitz) so $\lim_{t\to\infty} \| e^{\mathbf{A}t} \|_2 = 0$ and the steady-state part of the system's solution is

$$\begin{aligned}\mathbf{z}_{ss}(t) &= -(w^2\mathbf{I} + \mathbf{A}^2)^{-1}(\mathbf{A}\boldsymbol{\eta} - w\boldsymbol{\rho})\sin(wt) \\ &\quad - (w^2\mathbf{I} + \mathbf{A}^2)^{-1}(\mathbf{A}\boldsymbol{\rho} + w\boldsymbol{\eta})\cos(wt).\end{aligned} \tag{57}$$

Moreover, if $u(t) = k_1\sin(w_1 t) + k_2\sin(w_2 t)$, then

$$\begin{aligned}u^3(t) &= \left(\frac{3}{2}k_1{k_2}^2 + \frac{3}{4}{k_1}^3\right)\sin(w_1 t) \\ &\quad + \left(\frac{3}{2}{k_1}^2 k_2 + \frac{3}{4}{k_2}^3\right)\sin(w_2 t) \\ &\quad + \frac{3}{4}{k_1}^2 k_2\sin(\Omega_{\boldsymbol{I}} t) \\ &\quad + \frac{3}{4}k_1{k_2}^2\sin((2w_2 - w_1)t) \\ &\quad - \frac{3}{4}{k_1}^2 k_2\sin((2w_1 + w_2)t) \\ &\quad - \frac{3}{4}k_1{k_2}^2\sin((2w_2 + w_1)t) \\ &\quad - \frac{1}{4}{k_1}^3\sin(3w_1 t) - \frac{1}{4}{k_2}^3\sin(3w_2 t)\end{aligned} \tag{58}$$

where $\Omega_{\boldsymbol{I}} = 2w_1 - w_2$. Substituting (58) in (19) and superimposing the solutions of (19) for each of the frequencies in (58), implies that (59), shown at the bottom of the next page, is true.

Definition (16) and expression (59) provide that

$$\begin{aligned}\hat{y}_{\ell\ell n}(t) &= -\left(\frac{3}{2}k_1{k_2}^2 + \frac{3}{4}{k_1}^3\right)\alpha\mathbf{c}^T({w_1}^2\mathbf{I} + \mathbf{A}^2)^{-1} \\ &\quad \times (\mathbf{A}\mathbf{b}\sin(w_1 t) + w_1\mathbf{b}\cos(w_1 t)) \\ &\quad - \left(\frac{3}{2}{k_1}^2 k_2 + \frac{3}{4}{k_2}^3\right)\alpha\mathbf{c}^T({w_2}^2\mathbf{I} + \mathbf{A}^2)^{-1} \\ &\quad \times (\mathbf{A}\mathbf{b}\sin(w_2 t) + w_2\mathbf{b}\cos(w_2 t)) \\ &\quad - \frac{3}{4}{k_1}^2 k_2\alpha\mathbf{c}^T\left(\Omega_{\boldsymbol{I}}^2\mathbf{I} + \mathbf{A}^2\right)^{-1}\mathbf{A}\mathbf{b}\sin(\Omega_{\boldsymbol{I}} t) \\ &\quad - \frac{3}{4}{k_1}^2 k_2\alpha\mathbf{c}^T\left(\Omega_{\boldsymbol{I}}^2\mathbf{I} + \mathbf{A}^2\right)^{-1}\Omega_{\boldsymbol{I}}\mathbf{b}\cos(\Omega_{\boldsymbol{I}} t)\end{aligned} \tag{60}$$

APPENDIX C

The third Hadamard power of the vector[9]

$$\mathbf{x}(t) = \mathbf{h_1}\sin(w_1 t) + \mathbf{p_1}\cos(w_1 t) + \mathbf{h_2}\sin(w_2 t) + \mathbf{p_2}\cos(w_2 t) \tag{61}$$

is given by expression (62), shown at the bottom of the page.

APPENDIX D
STEPS TO DERIVE IM_3

1) *Derive the state-space description of the G_m-C filter.* Derive matrices $\mathbf{A}, \mathbf{b}$ and $\mathbf{c}$ of the ideal (linear) filter. Derive nonlinearity parameter α of the transconductors, analytically (Appendix A), or by fitting a third-order polynomial to the I–V characteristic of the transconductors.
2) *Form the input signal $u(t)$.* Choose the amplitudes k_1, k_2 and the frequencies w_1, w_2 of the input signal $u(t) = k_1\sin(w_1 t) + k_2\sin(w_2 t)$.
3) *Calculate $\tilde{\mathbf{h}}_\mathbf{1}, \tilde{\mathbf{p}}_\mathbf{1}, \tilde{\mathbf{h}}_\mathbf{2}$ and $\tilde{\mathbf{p}}_\mathbf{2}$ using* (24)

$$\begin{aligned}\tilde{\mathbf{h}}_\mathbf{1} &= -\left(w_1^2\mathbf{I} + \mathbf{A}^2\right)^{-1}\mathbf{Ab}\\ \tilde{\mathbf{p}}_\mathbf{1} &= -\left(w_1^2\mathbf{I} + \mathbf{A}^2\right)^{-1} w_1\mathbf{b}\\ \tilde{\mathbf{h}}_\mathbf{2} &= -\left(w_2^2\mathbf{I} + \mathbf{A}^2\right)^{-1}\mathbf{Ab}\\ \tilde{\mathbf{p}}_\mathbf{2} &= -\left(w_2^2\mathbf{I} + \mathbf{A}^2\right)^{-1} w_2\mathbf{b}.\end{aligned}$$

4) *Calculate $\tilde{\mathbf{s}}_{\mathbf{2},-\mathbf{1}}$ and $\tilde{\mathbf{c}}_{\mathbf{2},-\mathbf{1}}$ using* (26)

$$\begin{aligned}\widetilde{\mathbf{s}}_{\mathbf{2},-\mathbf{1}} &= \widetilde{\mathbf{h}}_\mathbf{1}^{\bullet 2} \bullet \widetilde{\mathbf{h}}_\mathbf{2} + 2\widetilde{\mathbf{h}}_\mathbf{1} \bullet \widetilde{\mathbf{p}}_\mathbf{1} \bullet \widetilde{\mathbf{p}}_\mathbf{2} - \widetilde{\mathbf{p}}_\mathbf{1}^{\bullet 2} \bullet \widetilde{\mathbf{h}}_\mathbf{2}\\ \widetilde{\mathbf{c}}_{\mathbf{2},-\mathbf{1}} &= \widetilde{\mathbf{p}}_\mathbf{1}^{\bullet 2} \bullet \widetilde{\mathbf{p}}_\mathbf{2} + 2\widetilde{\mathbf{h}}_\mathbf{1} \bullet \widetilde{\mathbf{p}}_\mathbf{1} \bullet \widetilde{\mathbf{h}}_\mathbf{2} - \widetilde{\mathbf{h}}_\mathbf{1}^{\bullet 2} \bullet \widetilde{\mathbf{p}}_\mathbf{2}\end{aligned}$$

5) *Calculate* $\mathbf{F} \triangleq (\Omega_{\boldsymbol{I}}^2\mathbf{I} + \mathbf{A}^2)^{-1}$ as well as $S_{2,-1}$ and $C_{2,-1}$ using (37) and (38), which are replicated at the top of the next page for convenience. **Remark: Terms corresponding to linear or nonexisting stages of the filter must be ignored**.

[9] h_1, p_1, h_2 and p_2 are column vectors of size n.

$$\begin{aligned}y_{\ell\ell n}(t) = &-\left(\frac{3}{2}k_1{k_2}^2 + \frac{3}{4}{k_1}^3\right)\alpha\mathbf{c}^T({w_1}^2\mathbf{I} + \mathbf{A}^2)^{-1}(\mathbf{Ab}\sin(w_1 t) + w_1\mathbf{b}\cos(w_1 t))\\ &-\left(\frac{3}{2}{k_1}^2 k_2 + \frac{3}{4}{k_2}^3\right)\alpha\mathbf{c}^T({w_2}^2\mathbf{I} + \mathbf{A}^2)^{-1}(\mathbf{Ab}\sin(w_2 t) + w_2\mathbf{b}\cos(w_2 t))\\ &-\frac{3}{4}{k_1}^2 k_2\alpha\mathbf{c}^T\left(\Omega_{\boldsymbol{I}}^2\mathbf{I} + \mathbf{A}^2\right)^{-1}(\mathbf{Ab}\sin(\Omega_{\boldsymbol{I}} t) + \Omega_{\boldsymbol{I}}\mathbf{b}\cos(\Omega_{\boldsymbol{I}} t))\\ &-\frac{3}{4}k_1{k_2}^2\alpha\mathbf{c}^T((2w_2 - w_1)^2\mathbf{I} + \mathbf{A}^2)^{-1}(\mathbf{Ab}\sin((2w_2 - w_1)t) + (2w_2 - w_1)\mathbf{b}\cos((2w_2 - w_1)t))\\ &+\frac{3}{4}{k_1}^2 k_2\alpha\mathbf{c}^T((2w_1 + w_2)^2\mathbf{I} + \mathbf{A}^2)^{-1}(\mathbf{Ab}\sin((2w_1 + w_2)t) + (2w_1 + w_2)\mathbf{b}\cos((2w_1 + w_2)t))\\ &+\frac{3}{4}k_1{k_2}^2\alpha\mathbf{c}^T((2w_2 + w_1)^2\mathbf{I} + \mathbf{A}^2)^{-1}(\mathbf{Ab}\sin((2w_2 + w_1)t) + (2w_2 + w_1)\mathbf{b}\cos((2w_2 + w_1)t))\\ &+\frac{1}{4}{k_1}^3\alpha\mathbf{c}^T(9{w_1}^2\mathbf{I} + \mathbf{A}^2)^{-1}(\mathbf{Ab}\sin(3w_1 t) + 3w_1\mathbf{b}\cos(3w_1 t))\\ &+\frac{1}{4}{k_2}^3\alpha\mathbf{c}^T(9{w_2}^2\mathbf{I} + \mathbf{A}^2)^{-1}(\mathbf{Ab}\sin(3w_2 t) + 3w_2\mathbf{b}\cos(3w_2 t))\end{aligned} \tag{59}$$

$$\begin{aligned}\mathbf{x}(t)^{\bullet 3} = &\left(3/4\mathbf{h_1} \bullet \mathbf{p_1}^{\bullet 2} + 3/2\mathbf{h_1} \bullet \mathbf{h_2}^{\bullet 2} + 3/2\mathbf{h_1} \bullet \mathbf{p_2}^{\bullet 2} + 3/4\mathbf{h_1}^{\bullet 3}\right)\sin(w_1 t)\\ &+\left(3/4\mathbf{h_1}^{\bullet 2} \bullet \mathbf{p_1} + 3/4\mathbf{p_1}^{\bullet 3} + 3/2\mathbf{p_1} \bullet \mathbf{h_2}^{\bullet 2} + 3/2\mathbf{p_1} \bullet \mathbf{p_2}^{\bullet 2}\right)\cos(w_1 t)\\ &+\left(3/4\mathbf{h_2} \bullet \mathbf{p_2}^{\bullet 2} + 3/2\mathbf{p_1}^{\bullet 2} \bullet \mathbf{h_2} + 3/4\mathbf{h_2}^{\bullet 3} + 3/2\mathbf{h_1}^{\bullet 2} \bullet \mathbf{h_2}\right)\sin(w_2 t)\\ &+\left(3/4\mathbf{h_2}^{\bullet 2} \bullet \mathbf{p_2} + 3/4\mathbf{p_2}^{\bullet 3} + 3/2\mathbf{p_1}^{\bullet 2} \bullet \mathbf{p_2} + 3/2\mathbf{h_1}^{\bullet 2} \bullet \mathbf{p_2}\right)\cos(w_2 t)\\ &+\left(3/4\mathbf{h_1}^{\bullet 2} \bullet \mathbf{h_2} + 3/2\mathbf{h_1} \bullet \mathbf{p_1} \bullet \mathbf{p_2} - 3/4\mathbf{p_1}^{\bullet 2} \bullet \mathbf{h_2}\right)\sin(\Omega_{\boldsymbol{I}} t)\\ &+\left(-3/4\mathbf{h_1}^{\bullet 2} \bullet \mathbf{p_2} + 3/2\mathbf{h_1} \bullet \mathbf{p_1} \bullet \mathbf{h_2} + 3/4\mathbf{p_1}^{\bullet 2} \bullet \mathbf{p_2}\right)\cos(\Omega_{\boldsymbol{I}} t)\\ &+\left(-3/4\mathbf{h_1} \bullet \mathbf{h_2}^{\bullet 2} + 3/4\mathbf{h_1} \bullet \mathbf{p_2}^{\bullet 2} - 3/2\mathbf{p_1} \bullet \mathbf{h_2} \bullet \mathbf{p_2}\right)\sin((w_1 - 2w_2)t)\\ &+\left(-3/4\mathbf{p_1} \bullet \mathbf{h_2}^{\bullet 2} + 3/2\mathbf{h_1} \bullet \mathbf{h_2} \bullet \mathbf{p_2} + 3/4\mathbf{p_1} \bullet \mathbf{p_2}^{\bullet 2}\right)\cos((w_1 - 2w_2)t)\\ &+\left(3/4\mathbf{p_1}^{\bullet 2} \bullet \mathbf{h_2} + 3/2\mathbf{h_1} \bullet \mathbf{p_1} \bullet \mathbf{p_2} - 3/4\mathbf{h_1}^{\bullet 2} \bullet \mathbf{h_2}\right)\sin((w_2 + 2w_1)t)\\ &+\left(3/4\mathbf{p_1}^{\bullet 2} \bullet \mathbf{p_2} - 3/4\mathbf{h_1}^{\bullet 2} \bullet \mathbf{p_2} - 3/2\mathbf{h_1} \bullet \mathbf{p_1} \bullet \mathbf{h_2}\right)\cos((w_2 + 2w_1)t)\\ &+\left(-3/4\mathbf{h_1} \bullet \mathbf{h_2}^{\bullet 2} + 3/4\mathbf{h_1} \bullet \mathbf{p_2}^{\bullet 2} + 3/2\mathbf{p_1} \bullet \mathbf{h_2} \bullet \mathbf{p_2}\right)\sin((w_1 + 2w_2)t)\\ &+\left(3/4\mathbf{p_1} \bullet \mathbf{p_2}^{\bullet 2} - 3/2\mathbf{h_1} \bullet \mathbf{h_2} \bullet \mathbf{p_2} - 3/4\mathbf{p_1} \bullet \mathbf{h_2}^{\bullet 2}\right)\cos((w_1 + 2w_2)t)\\ &+\left(-1/4\mathbf{h_1}^{\bullet 3} + 3/4\mathbf{h_1} \bullet \mathbf{p_1}^{\bullet 2}\right)\sin(3w_1 t)\\ &+\left(-3/4\mathbf{h_1}^{\bullet 2} \bullet \mathbf{p_1} + 1/4\mathbf{p_1}^{\bullet 3}\right)\cos(3w_1 t)\\ &+\left(3/4\mathbf{h_2} \bullet \mathbf{p_2}^{\bullet 2} - 1/4\mathbf{h_2}^{\bullet 3}\right)\sin(3w_2 t)\\ &+\left(-3/4\mathbf{h_2}^{\bullet 2} \bullet \mathbf{p_2} + 1/4\mathbf{p_2}^{\bullet 3}\right)\cos(3w_2 t)\end{aligned} \tag{62}$$

$$S_{2,-1} = \underbrace{-\mathbf{c}^T\mathbf{F}\mathbf{A}\mathbf{b}}_{\text{input}} \underbrace{-\mathbf{c}^T\mathbf{F}(\mathbf{A}^2\tilde{\mathbf{s}}_{\mathbf{2},-\mathbf{1}} - \Omega_{\boldsymbol{I}}\mathbf{A}\tilde{\mathbf{c}}_{\mathbf{2},-\mathbf{1}})}_{\text{filter core}} \underbrace{+\mathbf{c}^T\tilde{\mathbf{s}}_{\mathbf{2},-\mathbf{1}}}_{\text{output}}$$

$$C_{2,-1} = \underbrace{-\Omega_{\boldsymbol{I}}\mathbf{c}^T\mathbf{F}\mathbf{b}}_{\text{input}} \underbrace{-\mathbf{c}^T\mathbf{F}(\mathbf{A}^2\tilde{\mathbf{c}}_{\mathbf{2},-\mathbf{1}} + \Omega_{\boldsymbol{I}}\mathbf{A}\tilde{\mathbf{s}}_{\mathbf{2},-\mathbf{1}})}_{\text{filter core}} \underbrace{+\mathbf{c}^T\tilde{\mathbf{c}}_{\mathbf{2},-\mathbf{1}}}_{\text{output}}.$$

$$\mathcal{J}(w_1, w_2) = \sqrt{\frac{(S_{2,-1})^2 + (C_{2,-1})^2}{w_1^2\left(\mathbf{c}^T\left(w_1^2\mathbf{I} + \mathbf{A}^2\right)^{-1}\mathbf{b}\right)^2 + \left(\mathbf{c}^T\left(w_1^2\mathbf{I} + \mathbf{A}^2\right)^{-1}\mathbf{A}\mathbf{b}\right)^2}}$$

---

6) *Calculate* $\mathcal{J}(w_1, w_2)$ *using* (46), we obtain the second equation shown at the top of the page.
7) *Calculate* IM_3 *relatively to frequency component at* w_1 *using* (45)

$$\mathrm{IM}_3 \approxeq |\alpha|\frac{3k_1k_2}{4}\mathcal{J}(w_1, w_2).$$

References

[1] Y. Tsividis, "Integrated continuous-time filter design—An overview," *IEEE J. Solid-State Circuits*, vol. 29, no. 3, pp. 166–176, Mar. 1994.

[2] K. W. Moulding, J. R. Quartly, P. J. Rankin, R. J. Thompson, and G. A. Wilson, "Gyrator video filter IC with automatic tuning," *IEEE J. Solid-State Circuits*, vol. SC-15, no. 6, pp. 963–968, Dec. 1980.

[3] J. 0. Voorman, W. H. A. BNs, and P. J. Barth, "Integration of analog filters in bipolar process," *IEEE J. Solid-State Circuits*, vol. SC-17, no. 4, pp. 713–722, Aug. 1982.

[4] J. Silva-Martinez, "A 10.7 MHz 68-dB SNR CMOS continuous-time filter with on-chip automatic tuning," *IEEE J. Solid-State Circuits*, vol. 27, no. SC-12, pp. 1843–1853, Dec. 1992.

[5] A. Lewinski and J. Silva-Martinez, "OTA linearity enhancement technique for high-frequency applications with IM3 below -65 dB," *IEEE Trans. Circuits Syst. II, Exp. Briefs*, vol. 51, no. 10, pp. 542–548, Oct. 2004.

[6] T. H. Lee, *The Design of CMOS Radio-Frequency Integrated Circuits*. Cambridge, U.K.: Cambridge Univ. Press, 1998.

[7] D. A. Johns and K. Martin, *Analog Integrated Circuit Design*. New York: Wiley, 1997.

[8] J. E. Franca and Y. Tsividis, Eds., *Design of Analog-Digital VLSI Circuits for Telecommunications and Signal Processing*, 2nd ed. Englewood Cliffs, NJ: Prentice-Hall, 1994.

[9] P. Wambacq and W. Sansen, *Distortion Analysis of Analog Integrated Circuits*. Boston, MA: Kluwer, 1998.

[10] A. N. Mohieldin, E. Sanchez-Sinencio, and J. Silva-Martinez, "Nonlinear effects in pseudo differential OTAs with CMFB," *IEEE Trans. Circuits Syst. II, Analog Digit. Signal Process.*, vol. 50, no. 10, pp. 762–770, Oct. 2003.

[11] Y. Tsividis and J. O. Voorman, *Integrated Continuous-Time Filters*. New York: IEEE Press, 1993.

[12] Z. Y. Chang, "A highly linear CMOS G_m–C bandpass filter for video applications," in *Proc. IEEE Custom Integr. Circuits Conf.*, 1996, pp. 89–92.

[13] R. A. Baki, C. Beainy, and M. N. El-Gamal, "Distortion analysis of high-frequency log-domain filters using volterra series," *IEEE Trans. Circuits Syst. II, Analog Digit. Signal Process.*, vol. 50, no. 1, pp. 1–11, Jan. 2003.

[14] J. A. Cherry and W. M. Snelgrove, W. M., "On the characterization and reduction of distortion in bandpass filters," *IEEE Trans. Circuits Syst. I, Fundam. Theory Appl.*, vol. 45, no. 5, pp. 523–537, May 1998.

[15] S. Narayanan, "Application of volterra series to intermodulation distortion analysis of transistor feedback amplifiers," *IEEE Trans. Circuits Syst.*, vol. CAS-17, no. 11, pp. 518–527, Nov. 1970.

[16] B. Razavi, *RF Microelectronics*. Englewood Cliffs, NJ: Prentice-Hall, 1998.

[17] D. Pederson and K. Mayaram, *Analog Integrated Circuits for Communications*. Boston, MA: Kluwer, 1991.

[18] Y. Palaskas and Y. Tsividis, "Dynamic range optimization of weakly nonlinear fully balanced, G_m–C filters with power dissipation constraints," *IEEE Trans. Circuits Syst. II, Analog Digit. Signal Process.*, vol. 50, pp. 293–296, 2003.

[19] P. Kallam, E. Sanchez-Sinencio, and A. I. Karsilayan, "An enhanced adaptive Q-tuning scheme for a 100-MHz fully symmetric OTA-based bandpass filter," *IEEE J. Solid-State Circuits*, vol. 38, no. 4, pp. 585–593, Apr. 2003.

[20] J. Simmonds and J. Mann, Jr., *A First Look at Perturbation Theory*, 2nd ed. New York: Dover, 1997.

[21] T. Kato, *A Short Introduction to Perturbation Theory for Linear Operators*. New York: Springer-Verlag, 1982.

[22] T. Kato, *Perturbation Theory for Linear Operators*. New York: Springer-Verlag, 1995.

[23] T. Kailath, *Linear Systems*. Englewood Cliffs, NJ: Prentice-Hall, 1980.

[24] BSIM3 Version 3 Manual, BSIM Res. Gr., Dept, of Electr. Eng. Comp. Sci., Univ. of California, Berkeley, Sep. 1997 [Online]. Available: http://www-device.eecs.berkeley.edu/bsim3

[25] F. Bahmani and E. Sanchez-Sinencio, "A highly linear pseudo-differential transconductance," in *Proc. 30th Eur. Solid-State Circuits Conf. (ESSCIRC'04)*, Sep. 2004, pp. 111–114.

[26] Y. P. Tsividis and D. L. Fraser, "Harmonic distortion in single-channel MOS integrated circuits," *IEEE J. Solid-State Circuits*, vol. SC-16, no. 6, pp. 694–702, Dec. 1981.

[27] E. Fong and R. Zeman, "Analysis of harmonic distortion in single-channel MOS integrated circuits," *IEEE J. Solid-State Circuits*, vol. SC-17, no. 1, Feb. 1982.

[28] P. Wambacq, G. Gielen, P. Kinget, and W. Sansen, "High-frequency distortion analysis of analog integrated circuits," *IEEE Trans. Circuits Syst. II, Analog Digit. Signal Process.*, vol. 46, pp. 335–345, Mar. 1999.

[29] G. Palumbo and S. Pennisi, "High-frequency harmonic distortion in feedback amplifiers: Analysis and applications," *IEEE Trans. Circuits Syst. I, Fundam. Theory Appl.*, vol. 50, no. 3, pp. 328–340, Mar. 2003.

[30] S. Cannizzaro, G. Palumbo, and S. Pennisi, "Distortion analysis of Miller-compensated three-stage amplifiers," *IEEE Trans. Circuits Syst. I, Reg. Papers*, vol. 53, no. 5, pp. 961–976, May 2006.

[31] S. Cannizzaro, G. Palumbo, and S. Pennisi, "Accurate estimation of high-frequency harmonic distortion in two-stage Miller OTAs," *Proc. IEE Circuits Devices Syst.*, vol. 152, no. 5, pp. 417–424, Oct. 2005.

[32] S. Cannizzaro, G. Palumbo, and S. Pennisi, "Effects of nonlinear feedback in the frequency domain," *IEEE Trans. Circuits Syst. I, Reg. Papers*, vol. 53, no. 2, pp. 225–234, Feb. 2006.

[33] Y. Tsividis and J. O. Voorman, *Integrated Continuous-Time Filters*. New York: IEEE Press, 1993.

[34] Z. Zhang, A. Celik, and P. Sotiriadis, "State-space harmonic distortion modeling in weakly nonlinear, fully balanced G_m–C filters—A modular approach resulting in closed-form solutions," *IEEE Trans. Circuits Syst. I, Reg. Papers*, vol. 53, no. 1, pp. 48–59, Jan. 2006.

[35] P. Sotiriadis, A. Celik, and Z. Zhang, "Fast state-space harmonic distortion estimation in weakly nonlinear G_m–C filters," *IEEE Trans. Circuits Syst. I, Reg. Papers*, vol. 54, no. 1, pp. 218–228, Jan. 2007.

Abdullah Celik (S'03) received the B.S. degree in electrical and electronics engineering from the Bilkent University, Ankara, Turkey, and the M.S.E. degree from The Johns Hopkins University, Baltimore, MD, in 2002 and 2004, respectively.

He was a Research Assistant in the Adaptive Microsystems Laboratory at Johns Hopkins University. He is currently with MAXIM, Sunnyvale, CA. His research interests include the ultra low power design and implementation of custom VLSI systems for acoustical sensors, analog signal processing circuits and microelectromechanical system structures for audio reception.

Paul P. Sotiriadis (S'99–M'02) received the diploma in electrical engineering and computer science from the National Technical University of Athens (NTUA), Athens, Greece, the M.S. degree in electrical engineering from Stanford University, Stanford, CA, and the Ph.D. in electrical engineering and computer Science from the Massachusetts Institute of Technology, Cambridge, in 1996 and 2002, respectively.

Since June 2002, he has been an Assistant Professor in the Department of Electrical and Computer Engineering. The Johns Hopkins University, Baltimore, MD. His research interests include design, optimization, and mathematical modeling of analog and mixed-signal circuits, RF and microwave circuits, fine-frequency synthesis and interconnect networks in deep-submicrometer technologies.

Dr. Sotiriadis serves as an Associate Editor of the IEEE TRANSACTIONS ON CIRCUITS AND SYSTEMS—II: EXPRESS BRIEFS.

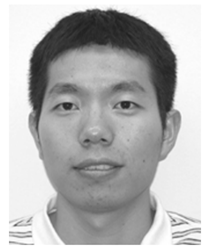

Zhaonian Zhang (S'02) received the B.S.E. degree in electronic engineering from Beijing Institute of Technology, Beijing, China, and the M.S.E. degree in electrical and computer engineering from The Johns Hopkins University, Baltimore, MD, in 2001 and 2004, respectively.

He is currently a Research Assistant in the Sensory Communications and Microsystems Lab at Johns Hopkins University. His current research interests include ultra-wide-band systems, microelectromechanical system structures for acoustic systems, and digital system design.

Mr. Zhang is a member of Tau Beta Pi.